NONLINEAR GUIDANCE AND CONTROL OF LEADER-FOLLOWER UAV FORMATIONS

A THESIS SUBMITTED TO
THE GRADUATE SCHOOL OF NATURAL AND APPLIED SCIENCES
OF
MIDDLE EAST TECHNICAL UNIVERSITY

BY

SARPER KUMBASAR

IN PARTIAL FULFILLMENT OF THE REQUIREMENTS
FOR
THE DEGREE OF MASTER OF SCIENCE
IN
AEROSPACE ENGINEERING

JANUARY 2015

Approval of the thesis:

NONLINEAR GUIDANCE AND CONTROL OF LEADER-FOLLOWER UAV FORMATIONS

submitted by **SARPER KUMBASAR** in partial fulfillment of the requirements for the degree of **Master of Science in Aerospace Engineering Department, Middle East Technical University** by,

Prof. Dr. Gülbin Dural Ünver ______________
Dean, Graduate School of **Natural and Applied Sciences**

Prof. Dr. Ozan Tekinalp ______________
Head of Department, **Aerospace Engineering**

Prof. Dr. Ozan Tekinalp ______________
Supervisor, **Aerospace Engineering Department, METU**

Examining Committee Members:

Prof. Dr. Aydan Erkmen
Electrical and Electronics Engineering Department, METU ______________

Prof. Dr. Ozan Tekinalp
Aerospace Engineering Department, METU ______________

Assoc. Prof. Dr. İlkay Yavrucuk
Aerospace Engineering Department, METU ______________

Assist. Prof. Dr. Ali Türker Kutay
Aerospace Engineering Department, METU ______________

Dr. Volkan Nalbantoğlu
Group Director, TAI ______________

Date: ______________

I hereby declare that all information in this document has been obtained and presented in accordance with academic rules and ethical conduct. I also declare that, as required by these rules and conduct, I have fully cited and referenced all material and results that are not original to this work.

Name, Last Name: SARPER KUMBASAR

Signature :

ABSTRACT

NONLINEAR GUIDANCE AND CONTROL OF LEADER-FOLLOWER UAV FORMATIONS

KUMBASAR, SARPER
M.S., Department of Aerospace Engineering
Supervisor : Prof. Dr. Ozan Tekinalp

January 2015, 72 pages

In this thesis work, two nonlinear guidance methods are proposed to control the autonomous formation flight: State Dependent Riccati Equation method and Lyapunov function method. Leader-Follower formation scheme is chosen and a pair of fighter aircrafts are used in simulations. One of them is chosen as the leader and it carries out the commanded maneuvers. Other aircraft is the follower and it follows the leader keeping the prescribed formation structure. Both aircraft models are nonlinear. In the inner loop, a nonlinear control algorithm, State Dependent Riccati Equation method is used to control the flight.

Keywords: Autonomous Formation Flight, SDRE, Lyapunov, Guidance, Leader-Follower Formation

ÖZ

İNSANSIZ HAVA ARACI LİDER-TAKİPÇİ KOL UÇUŞUNUN DOĞRUSAL OLMAYAN GÜDÜM VE KONTROLÜ

KUMBASAR, SARPER
Yüksek Lisans, Havacılık ve Uzay Mühendisliği Bölümü
Tez Yöneticisi : Prof. Dr. Ozan Tekinalp

Ocak 2015 , 72 sayfa

Bu çalışmada otonom kol uçuşu için iki tane doğrusal olmayan güdüm metodu geliştirilmiştir. Bu güdüm metodları; Duruma Bağlı Riccati Denklemi ve Lyapunov fonksiyonudur. Lider-Takipçi yapısında kol uçuşu simülasyonunda iki adet savaş uçağı kullanılmıştır. Uçaklardan biri lider olarak seçiliyor ve bu uçak verilen hız, baş açısı ve yükseklik komutlarını takip ediyor. Diğer uçak takipçi olarak seçiliyor ve lider uçağı belirli mesafeden takip ediyor. Kullanılan uçak modelleri doğrusal olmayan modellerdir. Ayrıca iki uçağın uçuş dinamikleri Duruma Bağlı Riccati Denklemi metodu ile kontrol edilmektedir.

Anahtar Kelimeler: Otonom Kol Uçuşu, Duruma Bağlı Riccati Denklemi, Lyapunov, Güdüm, Lider-Takipçi

Hayattaki en gerçek yol gösterici olan bilime

ACKNOWLEDGMENTS

I would like to thank to Prof. Dr. Ozan Tekinalp for his supervision. He enlarged my vision and showed me how I can contribute to science.

I also want to thank to my family for their supports.

Finally, I am thankful to Büşra Bartan for her supports.

TABLE OF CONTENTS

LIST OF FIGURES

FIGURES

NOMENCLATURE

h_R	Altitude of Reference Point, m
V_L, V_F	Velocity of Leader and Follower, m/s
γ_L, γ_F	Flight Path Angle of Leader and Follower
ψ_L, ψ_F	Heading of Leader and Follower
x_L, y_L, h_L	x, y and altitude Components of Leader Position, m
x_F, y_F, h_F	x, y and altitude Components of Follower Position, m
u, v, w	Body Velocity Components, m/s
p, q, r	Body Angular Velocity Components
ϕ, θ, ψ	Euler Angles
α	Angle of Attack
β	Side Slip Angle
m	Mass of Aircraft, kg
g	Gravitational Acceleration, m/s^2
C_T	Thrust Coefficient
a, b, c	Desired longitudinal, lateral, altitude distances respectively, m
C_X, C_Y, C_Z	Aerodynamic Coefficients in x,y,z body axis
C_l, C_m, C_n	Aerodynamic Roll, Pitch and Yaw Moment Coefficients

CHAPTER 1

INTRODUCTION

Usage of Unmanned Air Vehicles (UAVs) has grown in the past decade. One of the most important reason for that increase is related with the capabilities of UAVs that manned air vehicles do not have. With the UAVs, some missions that are not possible or not easy to do with human pilot has been made possible. For example, it is possible to make tight maneuvers with UAVs that high "g force" is desired but it is not possible because of the humans' limits. Also, UAVs can stay in air for days where it will be quite tiring for human pilot. There are also many other benefits that UAVs offer.

One of the most popular application with UAVs is the autonomous formation flight. Formation flight with proper formation structure can reduce the drag of the aircraft which is affected by the vortex produced from the preceding aircraft such as flying migratory birds in V-Shaped structure. Aerodynamic benefits of formation flight have been known for a long time and detailed information about aerodynamic benefits of the formation flight is given in [17]. On the other hand, aerial refuelling requires formation flight which may be done in an autonomous flight. Moreover, flying in formation long hours may impose extreme workload on pilots and may be alleviated by autonomous flight as well. On the other hand, it is believed that in the future, autonomous formation flight will be used widely for surveillance and reconnaissance missions in military applications.

In this study autonomous formation flight is investigated. Two nonlinear guidance algorithms are developed to control the formation flight in *Leader-Follower* approach. These algorithms use State Dependent Riccati Equation (SDRE) and Lyapunov methods. On the other hand, a new formation kinematics is derived and used in Leader

Fixed Frame. Moreover, flight controller is also designed with SDRE method and it is used in leader and follower aircraft. Proposed flight control and formation control algorithms are tested with simulations. However, the vortex effect to the follower aircraft produced by the leader is not modelled and expected to be addressed in a future work.

1.1 Literature Survey

In the literature, there are many different approaches to the autonomous formation flight. One of the most common is the *Leader-Follower* approach. In *Leader-Follower* structure, there is an aircraft which leads others and it is named as leader. Other aircrafts in the formation, try to keep the position in the formation scheme according to the information taken from the leader. Therefore, leader does not make any maneuver to keep the formation structure. According to [10], *Leader-Follower* structure may be separated into two modes such as *Leader Mode* and *Front Mode*, it is illustrated in Fig. 1.1. In *Leader Mode*, every aircraft takes the information from leader but in *Front Mode*, every aircraft takes the information from preceding one. Disadvantage of the *Front Mode* is that error propagation may occur through the rear aircraft. However, because of every aircraft in the formation taking the information from the leader, there is not error propagation problem. On the other hand, an advantage of the *Front Mode* is that collision avoidance may be easier to realize since every aircraft takes the information from preceding one. In [12], *Leader-Follower* approach is tested on radio controlled aircrafts built and designed at West Virginia University. In another study [23], micro air vehicles are used in *Leader-Follower* scheme.

Another method is the *Behavioral Approach* [11]. In this method, aircraft in the formation cooperate with each other. In that respect, it is different from *Leader-Follower* approach. For example, if one aircraft can not keep its relative position, all other aircrafts in the formation respond together to keep formation. However, there is not much work on this method in the literature.

In *Virtual structure* method, formation structure is considered as a rigid body and there is an imaginary point in the structure which is followed by all aircraft. There-

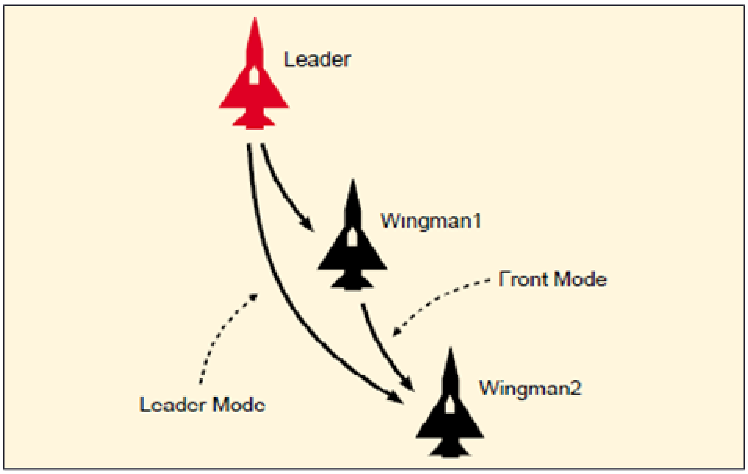

Figure 1.1: Leader and Front Mode [10]

fore, every aircraft in the formation takes the same signal. In [13], this method is tested in real flight. In the literature, other methods are also proposed. However, in this thesis work, *Leader-Follower* approach is selected and guidance algorithms are developed according to that. One of the reasons of this selection is that *Leader-Follower* approach is relatively simple to implement and easier to test with a pair of aircrafts in real tests.

There are popular guidance methods such as *proportional navigation* and *pursuit guidance* are used in missiles pursuit problems. These methods are used to go to a point but they are not suitable to stay at a relative position with respect to that point. In the literature classical "PID" or "LQR" controllers are used in formation flight. Although, they are successful to control the formation flight, nonlinear controllers have some advantages since they do not need trimming, linearization and gain scheduling. Also, nonlinear controllers can give better performance than linear controllers especially in highly nonlinear systems.

In this study, SDRE method is used to design both aircraft flight and formation flight controllers. SDRE is a nonlinear control method with growing popularity in last decade. This method was first proposed by [18], and later extended by Wernli and Cook [22]. Number of applications of the SDRE method in the flight control area exist in the literature. For example, it has been applied to control the aircraft flight [19], satellite attitude control [7], missile flight control [14], [15] and helicopter control

[3]. On the other hand, in [2], formation flight controller with SDRE method is also proposed.

Other method is the Lyapunov method. In [2], formation flight is also designed with Lyapunov method but in that work, there are singularity problems.

1.2 Contribution of the Thesis

In this thesis work, two nonlinear guidance algorithms to control the formation flight are proposed. These algorithms are developed with SDRE and Lyapunov function. In [2], SDRE and Lyapunov function based formation controllers were developed. However, in that work used formation kinematics are taken from [6] and with that formation kinematics, proposed formation controllers have some singularity problems. In this thesis work, a new formation kinematics is derived which alleviates the singularity problems. On the other hand, in [2], proposed formation control algorithms control the formation in two dimension so it does not control the altitude channel. Yet, in this thesis work, vertical separation in formation flight is also controlled.

In this study, nonlinear aircraft models are used in the simulations with a nonlinear flight controller, using SDRE method and it is used in the leader and the follower aircraft.

1.3 Outline

In next section, mathematical model of the aircraft is given. In Chapter 3, flight control design with SDRE method is developed. SDRE and Lyapunov based formation controllers are presented in Chapters 4 and 5 respectively. In Chapter 6, sensitivity of the proposed methods are examined then, discussion and comparison between the proposed methods are given in Chapter 7. Finally, conclusion and future work is given.

CHAPTER 2

MATHEMATICAL MODEL OF THE AIRCRAFT

2.1 Introduction

In this chapter, mathematical model of the aircraft is presented. Firstly, coordinate systems used in this work are introduced. Then, nonlinear equations of motion and used aircraft platform are given.

2.2 Coordinate Systems

There are different coordinate systems are used in aerospace. Some vectors can be easily stated in some coordinate systems but may be hard to state in another coordinate system. Therefore, different coordinate systems are used to show vectors easily in that coordinate systems. However, when deriving equations of motion, all vectors must be in the same coordinate system. Which necessitates using coordinates transformation to transform vectors from one to another.

There are four coordinate systems are used in this work as follows,

Earth Coordinate System (ECS):
The Earth axis system is fixed to the Earth and its z axis towards the center of the Earth. Also, x and y axis point North and East respectively.

Body Coordinate System (BCS):
The body axis system is fixed to the aircraft and its origin is at the aircraft's center of gravity. Its x axis towards the nose of the aircraft and y axis is pointing the right

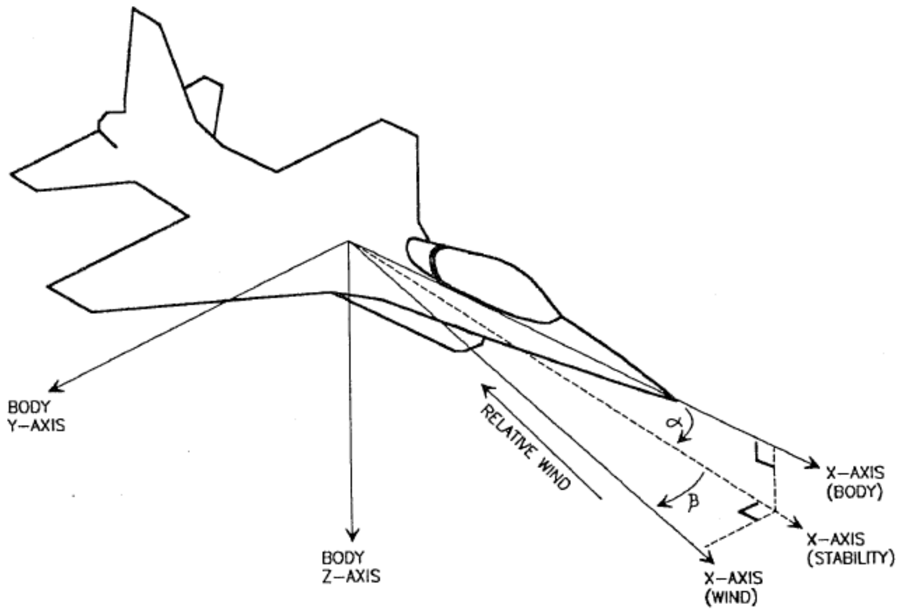

Figure 2.1: Coordinate Systems [20]

wing of the aircraft. Finally, z axis is determined with right hand rule. The coordinate system can be seen in Fig. 2.1.

Stability Coordinate System (SCS): As seen in Fig. 2.1, stability axis system is obtained with negative "α" (angle of attack) rotation around body y axis. This axis system is used for analysing the effect of perturbations from steady state flight.

Wind Coordinate System (WCS):
The wind axis system is obtained with positive β (sideslip angle) rotation around the stability z axis which aligns the wind x axis and relative wind.

2.3 Coordinate System Transformation

In this work, *euler rotation* method is used to transform a vector into another coordinate system. Another method is *quaternion* and further details about both method can be found in [20]. To transform from ECS to BCS is defined with coordinate transformation matrix as follows:

$$T_{BE} = \begin{bmatrix} cos\psi cos\theta & sin\psi cos\theta & -sin\theta \\ cos\psi sin\theta sin\phi - sin\psi cos\phi & sin\psi sin\theta sin\phi + cos\psi cos\phi & cos\theta sin\phi \\ cos\psi sin\theta cos\phi + sin\psi sin\phi & sin\psi sin\theta cos\phi - cos\psi sin\phi & cos\theta cos\phi \end{bmatrix} \tag{2.1}$$

Transformation matrix to transform from BCS to SCS:

$$T_{SB} = \begin{bmatrix} cos\alpha & 0 & sin\alpha \\ 0 & 1 & 0 \\ -sin\alpha & 0 & cos\alpha \end{bmatrix} \tag{2.2}$$

Transformation matrix to transform from SCS to WCS:

$$T_{WS} = \begin{bmatrix} cos\beta & sin\beta & 0 \\ -sin\beta & cos\beta & 0 \\ 0 & 0 & 1 \end{bmatrix} \tag{2.3}$$

2.4 Assumptions

Some simplifying assumptions are made in the simulations. First, aircraft is assumed rigid with constant mass density. Second, thrust is assumed to act along the X body axis and through the center of gravity. Third, earth's curvature is ignored and earth is assumed to be fixed in inertial space which means that its axes are inertial axes. Morevover, control surface deflections follow a standard right-hand rule sign convention, in which the fingers curl in the direction of positive control surface deflections when the thumb is pointed along the control surface hinge line in the direction of a positive body axis.

2.5 Nonlinear Equations of Motion

There are twelve equations used to describe the aircraft motion in this work. First group equations are derived according to Newton's second law and they are given in Eq. 2.4. The first group equations define the translational motion and they are given as body accelerations. When they are integrated, velocity of aircraft in body coordinate system is obtained.

$$\begin{aligned} \dot{u} &= rv - qw - gsin\theta + \frac{\bar{q}SC_x + T}{m} \\ \dot{v} &= pw - ru + gcos\theta sin\phi + \frac{\bar{q}SC_y}{m} \\ \dot{w} &= qu - pv + gcos\theta cos\phi + \frac{\bar{q}SC_z}{m} \end{aligned} \tag{2.4}$$

Second group equations define the rotational motion and they are given in Eq. 2.5. These equations are given as first derivative of body angular rates.

$$\begin{aligned} \dot{p} &= (C_1 r + C_2 p)q + \bar{q}Sb(C_3 C_l + C_4 C_n) \\ \dot{q} &= C_5 pr - C_6(p^2 - r^2) + \bar{q}S\bar{c}C_7 C_m \\ \dot{r} &= (C_8 p - C_2 r)q + \bar{q}Sb(C_4 C_l + C_9 C_n) \end{aligned} \tag{2.5}$$

Third group of equations are given in Eq. 2.6. These equations are first derivative of euler angles. They are integrated throughout the simulation and euler angles are obtained.

$$\begin{aligned} \dot{\phi} &= p + \tan\theta(q\sin\phi + r\cos\phi) \\ \dot{\theta} &= q\cos\phi - r\sin\phi \\ \dot{\psi} &= \frac{q\sin\phi + r\cos\phi}{\cos\theta} \end{aligned} \tag{2.6}$$

Last group equations give the velocity of aircraft in Earth coordinate system and they are integrated to find the position of aircraft in the Earth coordinate system. These equation are given in Eq. 2.7.

$$\begin{aligned} \dot{x}_E &= u\ cos\psi\ cos\theta + v\ (cos\psi\ sin\theta\ sin\phi - sin\psi\ cos\phi) \\ &\quad + w\ (cos\psi\ sin\theta\ cos\phi + sin\psi\ sin\phi) \\ \dot{y}_E &= u\ sin\psi\ cos\theta + v\ (sin\psi\ sin\theta\ sin\phi + cos\psi\ cos\phi) \\ &\quad + w\ (sin\psi\ sin\theta\ cos\phi - cos\psi\ sin\phi) \\ \dot{h}_E &= u\ sin\theta - v\ cos\theta\ sin\phi - w\ cos\theta\ cos\phi \end{aligned} \tag{2.7}$$

Given twelve equations can be found in [9]. Also, the coefficients C_1 to C_9 in 2.5 which are related with inertial terms given in same reference as follows:

$$\begin{aligned} & C_1 = \frac{(I_{yy} - I_{zz})I_{zz} - I_{xz}^2}{I_{xx}I_{zz} - I_{xz}^2}, \qquad C_2 = \frac{(I_{xx} - I_{yy} + I_{zz})I_{xz}}{I_{xx}I_{zz} - I_{xz}^2}, \\ & C_3 = \frac{I_{zz}}{I_{xx}I_{zz} - I_{xz}^2}, \qquad C_4 = \frac{I_{xz}}{I_{xx}I_{zz} - I_{xz}^2}, \\ & C_5 = \frac{(I_{zz} - I_{xx})}{I_{yy}}, \qquad C_6 = \frac{I_{xz}}{I_y}, \\ & C_7 = \frac{1}{I_y}, \qquad C_8 = \frac{(I_{xx} - I_{yy})I_{xx} - I_{xz}^2}{I_{xx}I_{zz} - I_{xz}^2}, \\ & C_9 = \frac{I_{xx}}{I_{xx}I_{zz} - I_{xz}^2} \end{aligned} \tag{2.8}$$

2.6 Platform

In this work, the McDonnell Douglas F-4 is used to test the proposed control methods. F-4 is a two-seat all-weather fighter/bomber aircraft. Thrust is provided by two General Electric GE-J19-17 afterburning jet engines mounted at the rear of the fuselage. Elevator deflection limits are $-21 \leq \delta_e \leq 7$, aileron deflection limits are $-15.5 \leq \delta_a \leq 15.5$, and rudder deflection limits are $-30 \leq \delta_r \leq 30$.

Other parameters of F-4: mass is 38924 lb, I_X is 24970 $slug.ft^2$, I_Y is 122190 $slug.ft^2$, I_Z is 139800 $slug.ft^2$, I_{XZ} is 1175 $slug.ft^2$. Wing span is 38.4 ft, wing reference area is 49.2 m^2.

2.7 Aerodynamic Model

Aerodynamic model of F-4 aircraft is taken from [9]. Aerodynamic model is very important part of designing SDC matrices. The model is given below for $\alpha \leq 15°$:

$$\begin{aligned} C_X = & -0.0434 + 2.39 \times 10^{-3}\alpha + 2.53 \times 10^{-5}\beta^2 - 1.07 \times 10^{-6}\alpha\beta^2 \\ & + 9.5 \times 10^{-4}\delta_e - 8.5 \times 10^{-7}\delta_e\beta^2 \\ & + \left(\frac{180q\bar{c}}{\pi 2V_t}\right)(8.73 \times 10^{-3} + 0.001\alpha - 1.75 \times 10^{-4}\alpha^2) \end{aligned} \tag{2.9}$$

$$
\begin{aligned}
C_Y = &- 0.012\beta + 1.55 \times 10^{-3}\delta_r - 8 \times 10^{-6}\delta_r\alpha \\
&+ \left(\frac{180\bar{b}}{\pi 2V_t}\right)(2.25 \times 10^{-3}p + 0.0117r - 3.67 \times 10^{-4}r\alpha + 1.75 \times 10^{-4}r\delta_e)
\end{aligned} \tag{2.10}
$$

$$
\begin{aligned}
C_Z = &- 0.131 - 0.0538\alpha - 4.76 \times 10^{-3}\delta_e - 3.3 \times 10^{-5}\delta_e\alpha - 7.5 \times 10^{-5}\delta_a^2 \\
&+ \left(\frac{180q\bar{c}}{\pi 2V_t}\right)(-0.111 + 5.17 \times 10^{-3}\alpha - 1.1 \times 10^{-3}\alpha^2)
\end{aligned} \tag{2.11}
$$

$$
\begin{aligned}
C_l = &- 5.98 \times 10^{-4}\beta - 2.83 \times 10^{-4}\alpha\beta + 1.51 \times 10^{-5}\alpha^2\beta \\
&- \delta_a(6.1 \times 10^{-4} + 2.5 \times 10^{-5}\alpha - 2.6 \times 10^{-6}\alpha^2) \\
&- \delta_r(-2.3 \times 10^{-4} + 4.5 \times 10^{-6}\alpha) \\
&+ \left(\frac{180\bar{b}}{\pi 2V_t}\right)(-4.12 \times 10^{-3}p - 5.24 \times 10^{-4}p\alpha + 4.36 \times 10^{-5}p\alpha^2 \\
&+ 4.36 \times 10^{-4}r + 1.05 \times 10^{-4}r\alpha + 5.24 \times 10^{-5}r\delta_e)
\end{aligned} \tag{2.12}
$$

$$
\begin{aligned}
C_m = &- 6.61 \times 10^{-3} - 2.67 \times 10^{-3}\alpha - 6.48 \times 10^{-5}\beta^2 - 2.65 \times 10^{-6}\alpha\beta^2 \\
&- 6.54 \times 10^{-3}\delta_e - 8.49 \times 10^{-5}\delta_e\alpha + 3.74 \times 10^{-6}\delta_e\beta^2 \\
&- 3.5 \times 10^{-5}\delta_a^2 + \left(\frac{180q\bar{c}}{\pi 2V_t}\right)(-0.0473 - 1.57 \times 10^{-3}\alpha)
\end{aligned} \tag{2.13}
$$

$$
\begin{aligned}
C_n = &\, 2.28 \times 10^{-3}\beta + 1.79 \times 10^{-6}\beta^3 + 1.4 \times 10^{-5}\delta_a \\
&+ 7.0 \times 10^{-6}\delta_a\alpha - 9.0 \times 10^{-4}\delta_r + 4.0 \times 10^{-6}\delta_r\alpha \\
&+ \left(\frac{180\bar{b}}{\pi 2V_t}\right)(-6.63 \times 10^{-5}p - 1.92 \times 10^{-5}p\alpha + 5.06 \times 10^{-6}p\alpha^2 \\
&- 6.06 \times 10^{-3}r - 8.73 \times 10^{-5}r\delta_e + 8.7 \times 10^{-6}r\delta_e\alpha)
\end{aligned} \tag{2.14}
$$

CHAPTER 3

FLIGHT CONTROLLER DESIGN WITH SDRE METHOD

3.1 Introduction

As stated in [5], "State Dependent Riccati Equation (SDRE) method has emerged as a very attractive tool for the systematic design of nonlinear controllers". Additionally, it is stated that it's popularity has increased within the control community over the last decade.

When designing a linear controller, it may be obtained the system matrix A and control matrix B. These are constant matrices for some trim points and obtained after linearization. Therefore, for other trim points these A and B matrices obtained again and gains are calculated for that trim point. Finally, with gain scheduling, linear controller can work at large flight envelope.

On the other hand, SDRE does not need linearization and gain scheduling because in SDRE method, system matrix A and control matrix B are not constant matrices. They are state dependent matrices and called as State Dependent Coefficient (SDC) matrices. These SDC matrices are updated at some hertz. After designing the SDC matrices, Linear Quadratic Regulator (LQR) and Linear Quadratic Tracking (LQT) can be used. In [19], LQR and LQT formulation is used, after SDC matrices design. The SDC matrices give extra design flexibility which is not seem in linear control methods [5].

3.2 SDRE Tracking Formulation

Given a linear dynamic system,

$$\begin{aligned} \dot{x}(t) &= A(t)x(t) + B(t)u(t) \\ y(t) &= C(t)x(t) \end{aligned} \tag{3.1}$$

where $x(t)$ is an n^{th} order state vector, $u(t)$ is the r^{th} order control vector, and $y(t)$ is the m^{th} order output vector. A trajectory tracking linear quadratic optimal control (LQT) can be formulated to control the system given in Eq. 3.1 such that the desired output $y(t)$ tracks the reference input $z(t)$ as close as possible while minimizing the following quadratic cost function [16, 1]:

$$J = \frac{1}{2}e^T(t_f)F(t_f)e(t_f) + \frac{1}{2}\int_{t_0}^{t_\infty} \left\{e^T(t)Q(t)e(t) + u^T(t)R(t)u(t)\right\} dt \tag{3.2}$$

where $e(t) = z(t) - y(t)$ is the error vector. It is assumed that $F(t_f)$ and $Q(t_f)$ are $m \times m$ symmetric positive semi-definite matrices, and $R(t)$ is an $r \times r$ symmetric positive definite matrix. In [19], another system is given in the form:

$$\begin{aligned} \dot{x}(t) &= A(t)x(t) + B(t)u(t) + f(t) \\ y(t) &= C(t)x(t) \end{aligned} \tag{3.3}$$

where $f(t)$ represents the mismatch that appears as a result of the factorization of the nonlinear system equations in the form of Eq. 3.1 provided that $f(t)$ is a slowly varying signal that may be assumed constant at certain time intervals, and f is bounded. If the performance index is defined by Eq. 3.13, the Hamiltonian then may be given as[19],

$$\begin{aligned} H(x(t), u(t), \lambda(t)) = {} & \tfrac{1}{2}\left[z(t) - C(t)x(t)\right]^T Q(t)\left[z(t) - C(t)x(t)\right] + \tfrac{1}{2}u^T(t)R(t)u(t) \\ & + \lambda^T(t)\left[A(t)x(t) + B(t)u(t) + f(t)\right] \end{aligned} \tag{3.4}$$

The optimal control is obtained from $\frac{\delta H}{\delta u} = 0$, which giving,

$$u^*(t) = -R^{-1}(t)B^T(t)\lambda^*(t) \tag{3.5}$$

The remaining equations for the states and costates can be obtained as,

$$\begin{bmatrix} \dot{x}^*(t) \\ \dot{\lambda}^*(t) \end{bmatrix} = \begin{bmatrix} A(t) & -E(t) \\ -V(t) & -A^{T(t)} \end{bmatrix} \begin{bmatrix} x^*(t) \\ \lambda^*(t) \end{bmatrix} + \begin{bmatrix} 0 \\ W(t) \end{bmatrix} z(t) + \begin{bmatrix} f(t) \\ 0 \end{bmatrix} \tag{3.6}$$

where

$$
\begin{aligned}
E(t) &= B(t)R^{-1}(t)B^T(t) \\
V(t) &= C^T(t)Q(t)C(t) \\
W(t) &= C^T(t)Q(t)
\end{aligned}
\tag{3.7}
$$

The boundary conditions for the state and costate equations are defined by the initial condition on the state: $x(t = t_0) = x(t_0)$ and the final condition on the costate:

$$
\lambda(t_f) = \frac{\delta}{\delta x(t_f)} \left[\frac{1}{2} e^T(t_f)F(t_f)e(t_f) \right] = C^T(t_f)F(t_f)C(t_f)x(t_f) - C^T(t_f)F(t_f)z(t_f) \tag{3.8}
$$

Assuming a linear relation between the state and co-state of the following form[16]:

$$
\lambda^*(t) = P(t)x^*(t) - g(t) \tag{3.9}
$$

where $P(t)$ is a square matrix size n and $g(t)$ is a vector of length n, are to be determined such that the canonical system (3.6) is satisfied. As a result it may be shown that if $P(t)$ can be found as solution to a matrix differential Riccati equation (3.10), and $g(t)$ is a solution to a vector differential equation (3.11):

$$
\dot{P}(t) = -P(t)A(t) - A^T(t)P(t) + P(t)E(t)P(t) - V(t) \tag{3.10}
$$

$$
\dot{g}(t) = \left[P(t)E(t) - A^T(t) \right] g(t) - W(t)z(t) + P(t)f(t) \tag{3.11}
$$

The optimal control is obtained in the form given by Eq. (3.12).

$$
u^*(t) = -R^{-1}(t)B^T(t)\left[P(t)x^*(t) - g(t) \right] = -K(t)x^*(t) + R^{-1}(t)B^T(t)g(t) \tag{3.12}
$$

For the infinite-horizon problem formulation, consider the system equation (3.3) but with the system matrices being time invariant, and the performance index chosen as

$$
\lim_{t_f \to \infty} J = \lim_{t_f \to \infty} \frac{1}{2} \int_{t_0}^{t_f} \left\{ e^T(t)Q(t)e(t) + u^T(t)R(t)u(t) \right\} dt \tag{3.13}
$$

Using the results for a finite-time case above and let $t_f \to \infty$ will lead to the infinite-time case solution. Thus, the matrix function $P(t)$ in Eq. 3.10 will result to the steady-state value P as the solution of the following algebraic Riccati equation:

$$
-PA - A^TP + PBR^{-1}B^TP - C^TQC = 0 \tag{3.14}
$$

For slowly varying input signals $z(t)$, solution of a matrix differential equation (3.11) can be obtained by setting the derivative to zero and solving Eq. 3.11 for $g(t)$:

$$
g(t) = \left[PE - A^T \right]^{-1} \left(Wz(t) + Pf(t) \right) \tag{3.15}
$$

where

$$\begin{aligned} E &= BR^{-1}B^T \\ W &= C^T Q \end{aligned} \tag{3.16}$$

Then the optimal control is:

$$u(t) = Kx(t) + K_z z(t) + K_f f(t) \tag{3.17}$$

and the corresponding controller gains are defined as:

$$\begin{aligned} K &= -R^{-1}B^T P \\ K_z &= R^{-1}B^T \left[PE - A^T\right]^{-1} W \\ K_f &= -R^{-1}B^T \left[PE - A^T\right]^{-1} P \end{aligned} \tag{3.18}$$

The nonlinear version of the optimal control may be realized using state dependent parametrization.

Consider a system is full state observable, autonomous, nonlinear in the state, and affine in the input, as given below[4]:

$$\dot{x}(t) = f(x) + B(x)u(t),\ x(0) = x_0 \tag{3.19}$$

where $x \in R^n$ is the state vector, $u \in R^m$ is the input vector, and $t \in [0, \infty)$, functions $f : R^n \to R^n$,
$B : R^n \to R^{n\times m}$ and $B(x) \neq 0, \forall x$.

First step of SDRE control design is SDC parametrization which means that a nonlinear system is being factorized into the linear-like structure containing SDC matrices [22, 8].

Under the assumptions $f(0) = 0$, and $f(\cdot) \in C^1(R^n)$ a continuous nonlinear matrix valued function A(x) always exists such that

$$f(x) = A(x)x \tag{3.20}$$

where A, the $n \times n$ matrix, is found by mathematical factorization and is nonunique when $n > 1$. Hence, extended linearization of the input-affine nonlinear system (3.19) becomes

$$\dot{x}(t) = A(x)x(t) + B(x)u(t), x(0) = x_0 \tag{3.21}$$

which has a linear structure with SDC matrices A(x), B(x). The application of any linear control synthesis method to the linear-like SDC structure $A(x)$ and $B(x)$ are treated as constant matrices, forms an extended linearization control method [4].

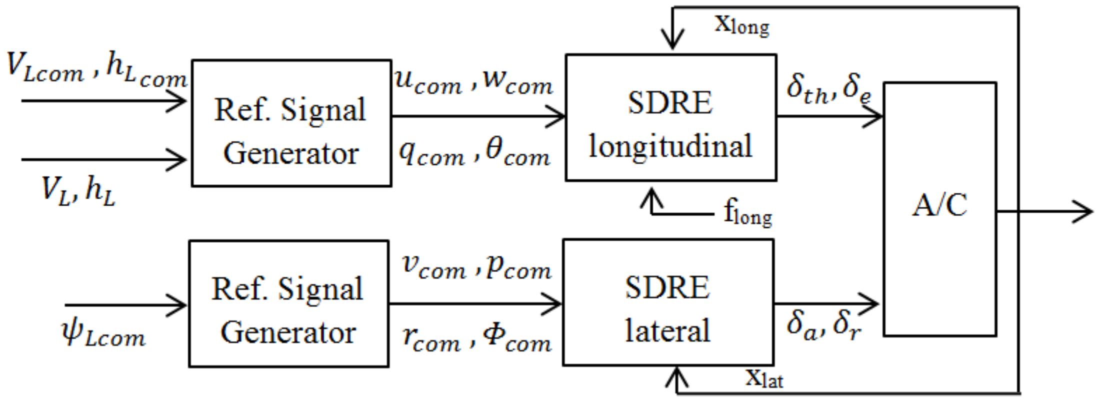

Figure 3.1: Leader Aircraft's General Control Layout with SDRE Method

3.3 Flight Control Design

In this study, leader and follower aircraft's flight controllers are designed with SDRE method. Follower has two loop structure as inner loop and outer loop. In inner loop, SDRE based flight controller works and outer loop controls the formation flight designed with SDRE and Lyapunov methods which are given in next sections. On the other hand, leader does not have an outer loop, it just has a flight controller.

In Fig. 3.1, leader aircraft's flight controller block diagram is given. According to block diagram, speed, altitude and heading commands are given to the leader and it carry outs the given maneuver commands. Firstly, given speed and altitude commands are send to Ref. Signal Generator block and this block performs trimming algorithm to generate u, w, q, θ signals. Then, these signals are send to SDRE longitudinal block diagram. Inside of the SDRE longitudinal block diagram is shown in Fig. 3.2 and this block will generate throttle and elevator signals. Similar to longitudinal channel, lateral channel takes heading command and it will generates aileron and rudder signals. Inside of the SDRE lateral block is given in Fig. 3.3. In the simulation, inner loop SDRE blocks are running at 5 hertz.

3.3.1 Longitudinal Channel

SDRE longitudinal control block diagram is given in Fig. 3.2. According to this figure, z_{long} represent the reference vector which consists of the longitudinal states will be tracked by the aircraft:

$$z_{long} = [u_{com},\ w_{com},\ q_{com},\ \theta_{com}]^T \tag{3.22}$$

x_{long} consists of the longitudinal states:

$$x_{long} = [u,\ w,\ q,\ \theta]^T \tag{3.23}$$

input will be throttle and elevator:

$$u_{long} = [\delta_{th},\ \delta_e]^T \tag{3.24}$$

Nonlinear system for the longitudinal motion,

$$\dot{x}_{long} = A_{long}x_{long} + B_{long}u_{long} + f_{long} \tag{3.25}$$

One term due to gravity, may not be put into SDC formulation. This term is included as an external slowly varying disturbance:

$$f_{long} = [0,\ g\cos(\theta)\cos(\phi),\ 0,\ 0]^T \tag{3.26}$$

For the cost function given below:

$$\lim_{t_f \to \infty} J = \lim_{t_f \to \infty} \frac{1}{2} \int_{t_0}^{t_f} \left\{ e^T(t)Qe(t) + u^T(t)Ru(t) \right\} dt \tag{3.27}$$

Where, $e_{long} = z_{long} - x_{long}$ and the optimal control will be:

$$u_{long} = Kx_{long} + K_z z_{long} + K_f f_{long} \tag{3.28}$$

The gains can be calculated with Eq. 3.18. The most important part of the control design of SDRE method is to design SDC matrices and the matrices are given below. Terms of the matrices mostly depends on the aerodynamic terms. It should be noted that SDC matrix design is not unique and alternative designs could be generated. Therefore, SDC matrices give extra design flexibility [5].

$$\begin{aligned} A_{long}(1,1) = \frac{\rho u}{2}\frac{S}{m}(&-0.0434 + 2.39 \times 10^{-3}\alpha + 2.53 \times 10^{-5}\beta^2 \\ &- 1.07 \times 10^{-6}\alpha\beta^2) \end{aligned} \tag{3.29}$$

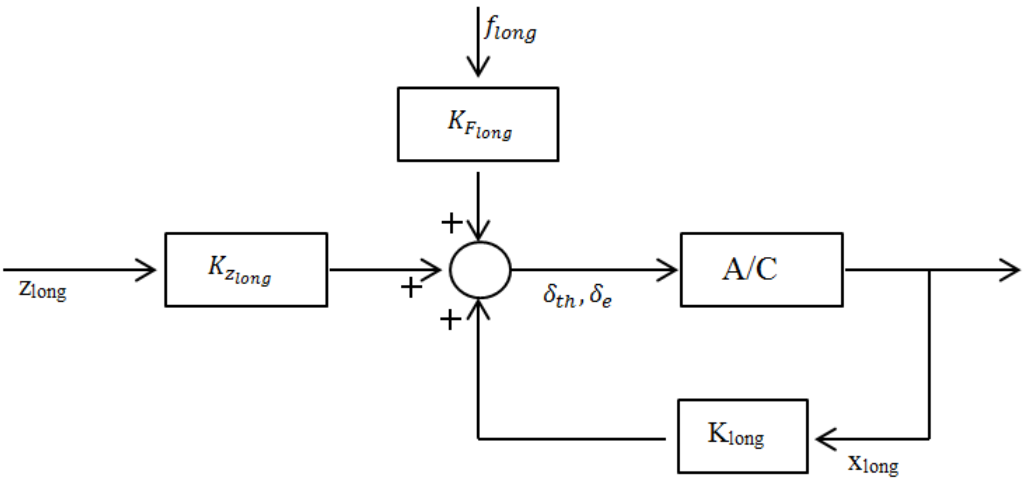

Figure 3.2: Control Block Diagram of Longitudinal Motion

$$A_{long}(1,2) = -\frac{q}{2} \tag{3.30}$$

$$A_{long}(1,3) = \frac{180\bar{c}}{2\pi V_t}(8.73 \times 10^{-3} + 0.001\alpha - 1.75 \times 10^{-4}\alpha^2)\frac{\bar{q}S}{m} - 0.5w \tag{3.31}$$

$$A_{long}(1,4) = -g\frac{\sin(\theta)}{\theta} \tag{3.32}$$

$$A_{long}(2,1) = -0.131 \times \frac{1}{2}\rho u\frac{S}{m} + 0.5q \tag{3.33}$$

$$A_{long}(2,2) = -0.0538 \times \frac{180}{\pi u}\bar{q}\frac{S}{m} \tag{3.34}$$

$$A_{long}(2,3) = \frac{180\bar{c}}{2\pi V_t}(-0.111 + 5.17 \times 10^{-3}\alpha - 1.1 \times 10^{-3}\alpha^2)\bar{q}\frac{S}{m} + 0.5u \tag{3.35}$$

$$A_{long}(2,4) = 0 \tag{3.36}$$

$$A_{long}(3,1) = \frac{1}{2}\rho uS\bar{c}C_7(-6.61 \times 10^{-3} - 6.48 \times 10^{-5}\beta^2 - 2.65 \times 10^{-6}\alpha\beta^2) \tag{3.37}$$

$$A_{long}(3,2) = -2.67 \times 10^{-3}\frac{1}{u}\frac{180}{\pi}\bar{q}S\bar{c}C_7 \tag{3.38}$$

$$A_{long}(3,3) = \frac{180\bar{c}}{2\pi V_t}(-0.0473 - 1.57 \times 10^{-3}\alpha)\bar{q}S\bar{c}C_7 \tag{3.39}$$

$$A_{long}(3,4) = 0 \tag{3.40}$$

$$A_{long}(4,1) = 0 \tag{3.41}$$

$$A_{long}(4,2) = 0 \tag{3.42}$$

$$A_{long}(4,3) = \cos\phi \tag{3.43}$$

$$A_{long}(4,4) = 0 \tag{3.44}$$

$$B_{long} = \begin{bmatrix} \frac{C_T}{m} & (9.5 \times 10^{-4} - 8.5 \times 10^{-7}\beta^2)\frac{\bar{q}S}{m} \\ 0 & (-4.76 \times 10^{-3} - 3.3 \times 10^{-5}\alpha)\frac{\bar{q}S}{m} \\ 0 & (-6.54 \times 10^{-3} - 8.49 \times 10^{-5}\alpha + 3.74 \times 10^{-6}\beta^2)\bar{q}S\bar{c}C_7 \\ 0 & 0 \end{bmatrix} \tag{3.45}$$

3.3.2 Lateral Channel

SDRE lateral control block diagram is given in Fig. 3.3. In this figure, z_{lat} represent the reference vector and it consists of the lateral states.

$$z_{lat} = [v_{com},\ p_{com},\ r_{com},\ \phi_{com}]^T \tag{3.46}$$

The reference vector z_{lat} will be tracked by the aircraft. Also, state vector x_{lat} is given:

$$x_{lat} = [v,\ p,\ r,\ \phi]^T \tag{3.47}$$

And input consists of the aileron and rudder signals.

$$u_{lat} = [\delta_a,\ \delta_r]^T \tag{3.48}$$

Similar to Eq. 3.25, the dynamics are given for the lateral channel:

$$\dot{x}_{lat} = A_{lat}x_{lat} + B_{lat}u_{lat} \tag{3.49}$$

There is no mismatch between the dynamics and SDC matrices so f_{lat} is not needed. For the same cost function given in Eq. 3.27, error signal is given as $e_{lat} = z_{lat} - x_{lat}$ and optimal control will be such that:

$$u_{lat} = Kx_{lat} + K_z z_{lat} \tag{3.50}$$

The gains in Eq. 3.50 can be calculated with Eq. 3.18. Finally, SDC matrices for lateral channel are given:

$$A_{lat}(1,1) = -0.012\frac{1}{V_t}\frac{180}{\pi}\frac{\bar{q}S}{m} \tag{3.51}$$

$$A_{lat}(1,2) = \frac{180\bar{b}}{2\pi V_t}(2.25 \times 10^{-3})\frac{\bar{q}S}{m} + w \tag{3.52}$$

$$A_{lat}(1,3) = \frac{180\bar{b}}{2\pi V_t}(0.0117 - 3.67 \times 10^{-4}\alpha + 1.75 \times 10^{-4}\delta_e)\frac{\bar{q}S}{m} - u \tag{3.53}$$

$$A_{lat}(1,4) = \frac{g\cos\theta\sin\phi}{\phi} \tag{3.54}$$

$$\begin{aligned} A_{lat}(2,1) = [&(-5.98 \times 10^{-4} - 2.83 \times 10^{-4}\alpha + 1.51 \times 10^{-5}\alpha^2)C_3 \\ &+ (2.28 \times 10^{-3} + 1.79 \times 10^{-6}\beta^2)C_4]\frac{180}{\pi V_t}\bar{q}S\bar{b} \end{aligned} \tag{3.55}$$

$$\begin{aligned} A_{lat}(2,2) = &[(-4.12 \times 10^{-3} - 5.24 \times 10^{-4}\alpha + 4.36 \times 10^{-5}\alpha^2)C_3 \\ &+ (-6.63 \times 10^{-5} - 1.92 \times 10^{-5}\alpha + 5.06 \times 10^{-6}\alpha^2)C_4]\frac{180\bar{b}}{2\pi V_t}\bar{q}S\bar{b} \\ &+ C_2 q \end{aligned} \tag{3.56}$$

$$\begin{aligned} A_{lat}(2,3) = &[(4.36 \times 10^{-4} + 1.05 \times 10^{-4}\alpha + 5.24 \times 10^{-5}\delta_e)C_3 \\ &+ (-6.06 \times 10^{-3} - 8.73 \times 10^{-5}\delta_e + 8.7 \times 10^{-6}\delta_e\alpha)C_4]\frac{180\bar{b}}{\pi 2V_t}\bar{q}S\bar{b} \\ &+ C_1 q \end{aligned} \tag{3.57}$$

$$A_{lat}(2,4) = 0 \tag{3.58}$$

$$\begin{aligned} A_{lat}(3,1) = [&(-5.98 \times 10^{-4} - 2.83 \times 10^{-4}\alpha + 1.51 \times 10^{-5}\alpha^2)C_4 \\ &+ (2.28 \times 10^{-3} + 1.79 \times 10^{-6}\beta^2)C_9]\bar{q}S\bar{b}\frac{180}{\pi V_t} \end{aligned} \tag{3.59}$$

$$\begin{aligned} A_{lat}(3,2) = &[(-4.12 \times 10^{-3} - 5.24 \times 10^{-4}\alpha + 4.36 \times 10^{-5}\alpha^2)C_4 \\ &+ (-6.63 \times 10^{-5} - 1.92 \times 10^{-5}\alpha + 5.06 \times 10^{-6}\alpha^2)C_9]\frac{180\bar{b}}{2\pi V_t}\bar{q}S\bar{b} \\ &+ C_8 q \end{aligned} \tag{3.60}$$

$$\begin{aligned} A_{lat}(3,3) = &[(4.36 \times 10^{-4} + 1.05 \times 10^{-4}\alpha + 5.24 \times 10^{-5}\delta_e)C_4 \\ &+ (-6.06 \times 10^{-3} - 8.73 \times 10^{-5}\delta_e + 8.7 \times 10^{-6}\delta_e\alpha)C_9]\frac{180\bar{b}}{2\pi V_t}\bar{q}S\bar{b} \\ &- C_2 q \end{aligned} \tag{3.61}$$

$$A_{lat}(3,4) = 0 \tag{3.62}$$

$$A_{lat}(4,1) = 0 \tag{3.63}$$

$$A_{lat}(4,2) = 1 \tag{3.64}$$

$$A_{lat}(4,3) = \tan\theta\cos\phi \tag{3.65}$$

$$A_{lat}(4,4) = \frac{q\tan\theta\sin\phi}{\phi} \tag{3.66}$$

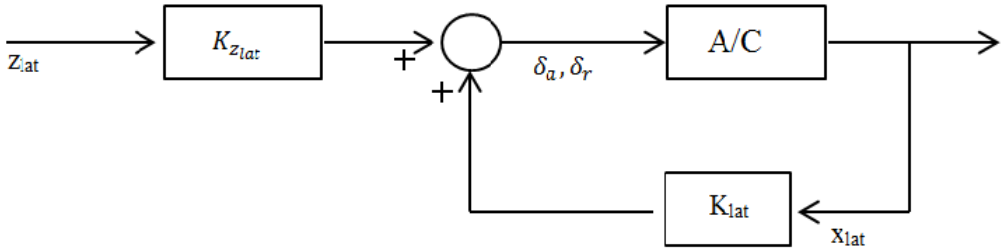

Figure 3.3: Control Block Diagram of Lateral Motion

$$B_{lat}(1,1) = 0 \tag{3.67}$$

$$B_{lat}(1,2) = (1.55 \times 10^{-3} - 8 \times 10^{-6}\alpha)\frac{\bar{q}S}{m} \tag{3.68}$$

$$\begin{aligned} B_{lat}(2,1) = {} & [(-6.1 \times 10^{-4} - 2.5 \times 10^{-5}\alpha + 2.6 \times 10^{-6}\alpha^2)C_3 \\ & + (1.4 \times 10^{-5} + 7 \times 10^{-6}\alpha)C_4]\bar{q}S\bar{b} \end{aligned} \tag{3.69}$$

$$B_{lat}(2,2) = [2.3\times 10^{-4} - 4.5\times 10^{-6}\alpha)C_3 + (-9\times 10^{-4} + 4\times 10^{-6}\alpha)C_4]\bar{q}S\bar{b} \tag{3.70}$$

$$\begin{aligned} B_{lat}(3,1) = {} & [(-6.1 \times 10^{-4} - 2.5 \times 10^{-5}\alpha + 2.6 \times 10^{-6}\alpha^2)C_4 \\ & + (1.4 \times 10^{-5} + 7 \times 10^{-6}\alpha)C_9]\bar{q}S\bar{b} \end{aligned} \tag{3.71}$$

$$B_{lat}(3,2) = [(2.3\times 10^{-4} - 4.5\times 10^{-6}\alpha)C_4 + (-9\times 10^{-4} + 4\times 10^{-6}\alpha)C_9]\bar{q}S\bar{b} \tag{3.72}$$

$$B_{lat}(4,1) = 0 \tag{3.73}$$

$$B_{lat}(4,2) = 0 \tag{3.74}$$

CHAPTER 4

FORMATION CONTROL WITH SDRE

4.1 Formation Kinematics

In this thesis work, a new formation kinematics is presented for the *Leader-Follower* formation structure. In this kinematics, *Leader Fixed Frame* is chosen. *Inertial Frame* and *Leader Fixed Frame* are given in Fig. 4.1. In this figure, according to the right hand rule, z axis is through the page. On the other hand, it is important to note that difference between the local vertical local horizontal frame, assumed to be inertial and the *Leader Fixed Frame* is mainly the heading angle of the leader aircraft. Although leader changes its roll and pitch angles, *Leader Fixed Frame* stays align with horizontal frame. According to the Fig. 4.1, "L" represents leader aircraft and "F" represent follower aircraft. Also, "R" represents reference point where the follower should be on through the formation flight. The point "R" is described as longitudinally "a", laterally "b" and vertically "c" distance away form the leader. Distance "c" is not showed in figure, it is in the positive z direction. On the other hand, d_{long} and d_{lat} is given in Fig. 4.1, they are formation errors in x-y plane and there is also $h_R - h_F$ distance represents the formation error in vertical. Therefore, d_{long}, d_{lat} and $h_R - h_F$ are desired to be zero. The formation equations are derived similar to reference [21]. Thus the following error vector is considered.

$$\overrightarrow{FR} = d_{long}\vec{i} + d_{lat}\vec{j} \tag{4.1}$$

where, $\vec{i}, \vec{j}, \vec{k}$ are the unit vectors attached to the leader aircraft. The derivative of $\overrightarrow{FR}$ may be written in two ways as,

$$\frac{d\overrightarrow{FR}}{dt} = \dot{d}_{long}\vec{i} + \dot{d}_{lat}\vec{j} + \dot{\psi}_L\vec{k} \times \left(d_{long}\vec{i} + d_{lat}\vec{j}\right) \tag{4.2}$$

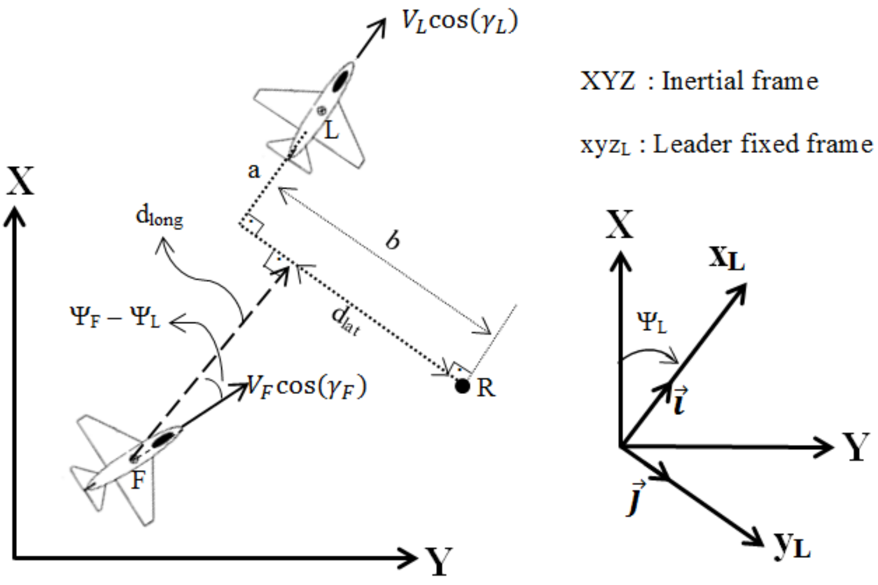

Figure 4.1: Formation Kinematics [21]

$$\frac{d\overrightarrow{FR}}{dt} = \overrightarrow{V_R}\,cos(\gamma_L) - \overrightarrow{V_F}\,cos(\gamma_F) \tag{4.3}$$

$\overrightarrow{V_R}\,cos(\gamma_L)$ is stated as:

$$\overrightarrow{V_R}\,cos(\gamma_L) = \overrightarrow{V_L}\,cos(\gamma_L) + \dot{\psi}_L\vec{k} \times \left(-a\vec{i} + b\vec{j}\right) \tag{4.4}$$

Eq. (4.4) is substituted into Eq. (4.3). Then, because of Eq. (4.2) and (4.3) are equivalent, following is obtained:

$$\dot{d}_{long}\vec{i} + \dot{d}_{lat}\vec{j} = \overrightarrow{V_L}\,cos(\gamma_L) - \overrightarrow{V_F}\,cos(\gamma_F) + \dot{\psi}_L\vec{k} \times \overrightarrow{LF} \tag{4.5}$$

After that $\overrightarrow{LF}$ in Leader Frame is given below:

$$\begin{aligned}\overrightarrow{LF} = &\{(X_F - X_L)\cos(\psi_L) + (Y_F - Y_L)\sin(\psi_L)\}\,\vec{i} \\ &+ \{-(X_F - X_L)\sin(\psi_L) + (Y_F - Y_L)\cos(\psi_L)\}\,\vec{j}\end{aligned} \tag{4.6}$$

Finally, the formation equations are obtained as:

$$\begin{aligned}\dot{d}_{long} &= V_L\,cos(\gamma_L) - V_F\,cos(\gamma_F)\,cos(\psi_F - \psi_L) - \dot{\psi}_L\,sin(\psi_L)\,(X_L - X_F) \\ &\quad + \dot{\psi}_L\,cos(\psi_L)\,(Y_L - Y_F) \\ \dot{d}_{lat} &= -V_F\,cos(\gamma_F)\,sin(\psi_F - \psi_L) - \dot{\psi}_L\,cos(\psi_L)\,(X_L - X_F) \\ &\quad - \dot{\psi}_L\,sin(\psi_L)\,(Y_L - Y_F) \\ \dot{h}_R - \dot{h}_F &= V_L\,sin(\gamma_L) - V_F\,sin(\gamma_F)\end{aligned} \tag{4.7}$$

4.2 Formation Control Design

To control the formation flight autonomously, SDRE regulator formulation is used [19]. Thus, we define a quadratic cost function:

$$J(x_0, u) = \frac{1}{2}\int_0^\infty \left\{x^T(t)Qx(t) + u^T(t)Ru(t)\right\} dt \tag{4.8}$$

where $Q(x) \in R^{n\times m}$ is symmetric positive semidefinite, $R(x) \in R^{m\times m}$ is symmetric positive definite matrix. The feedback gain is given:

$$u(x) = -K(x)x = -R^{-1}(x)B^T(x)P(x)x \tag{4.9}$$

$P(x)$ is the solution of the following Algebraic State Dependent Riccati Equation:

$$P(x)A(x)A^T(x)P(x) - P(x)B(x)R^{-1}(x)B^T(x)P(x) + Q(x) = 0 \tag{4.10}$$

Where $A(x)$ and $B(x)$ are the state dependent coefficient (SDC) matrices. If there is a mismatch term $f(t)$ in Eq.(4.11) between the Eq. (4.7) and SDC matrices. Therefore, feedback gain is modified as:

$$u(t) = Kx(t) + K_f f(t) \tag{4.11}$$

where K and K_f is given in Eq. (3.18). This formulation will drive d_{long}, d_{lat} and $(h_R - h_F)$ to zero. The formation equation is given below:

$$\dot{x}_{guide} = A_{guide}x_{guide} + B_{guide}u_{guide} + f_{guide} \tag{4.12}$$

According to the Eq. 4.12, the state vector which will be driven to zero is given:

$$x_{guide} = [d_{long},\ d_{lat},\ h_r - h_f]^T \tag{4.13}$$

And, SDC matrices are selected as:

$$A_{guide} = \begin{bmatrix} 0 & 0 & 0 \\ 0 & 0 & 0 \\ 0 & 0 & 0 \end{bmatrix} \tag{4.14}$$

$$B_{guide} = \begin{bmatrix} -\cos\gamma_F\ \cos(\psi_F - \psi_L) & 0 & 0 \\ -\frac{\cos\gamma_F\ \sin(\psi_F-\psi_L)}{2} & -\frac{V_F\ \sin(\psi_F-\psi_L)\cos\gamma_F}{2(\psi_F-\psi_L)} & 0 \\ -\frac{\sin\gamma_F}{2} & 0 & -\frac{V_F\sin\gamma_F}{2\gamma_F} \end{bmatrix} \tag{4.15}$$

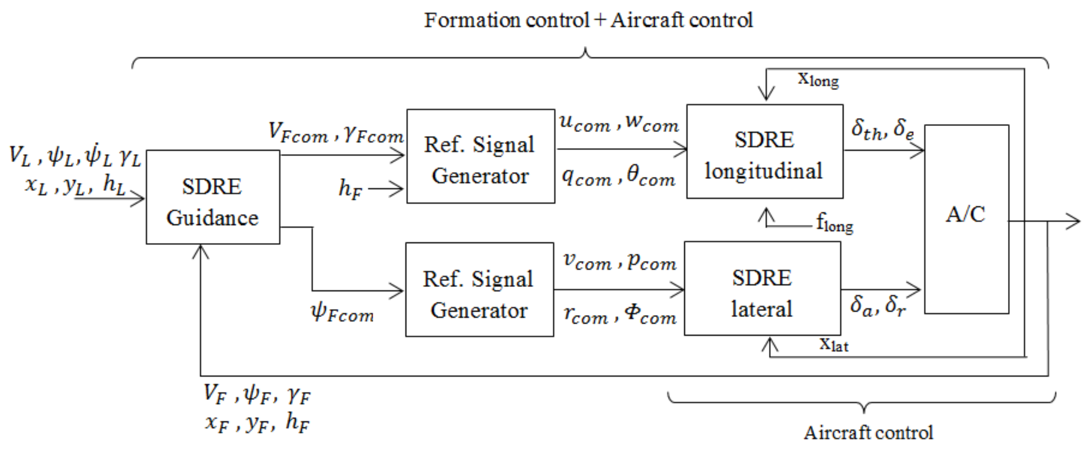

Figure 4.2: Follower Aircraft's Control Block Diagram with SDRE Method

Mismatch between Eq. (4.7) and SDC matrices is:

$$f_{guide} = \begin{bmatrix} V_L cos(\gamma_L) - \dot{\psi}_L\ sin(\psi_L)\ (x_L - x_F) + \dot{\psi}_L\ cos(\psi_L)\ (y_L - y_F) \\ -\dot{\psi}_L\ cos(\psi_L)\ (x_L - x_F) - \dot{\psi}_L\ sin(\psi_L)\ (y_L - y_F) \\ V_L\ sin(\gamma_L) \end{bmatrix} \tag{4.16}$$

Finally, input signal will be,

$$u_{guide} = [V_F,\ \psi_F - \psi_L,\ \gamma_F,]^T \tag{4.17}$$

The output of the guidance algorithm is u_{guide}. Here, u_{guide} has the term $\psi_F - \psi_L$ and because of the ψ_L has known parameter, ψ_F can be obtained easily. Then; V_F, ψ_F and γ_F commands are fed to the inner flight control loop of the follower aircraft. The block diagram is given in Fig 4.2. A blow up of the SDRE guidance block diagram is given in Fig. 4.3. The SDRE guidance algorithm works at 1 hz.

However, this formulation may result in small steady state errors but this may be alleviated by integral states. The new SDC matrices are given then:

$$A_{guide} = \begin{bmatrix} 0 & 1 & 0 & 0 & 0 \\ 0 & 0 & 0 & 0 & 0 \\ 0 & 0 & 0 & 1 & 0 \\ 0 & 0 & 0 & 0 & 0 \\ 0 & 0 & 0 & 0 & 0 \end{bmatrix} \tag{4.18}$$

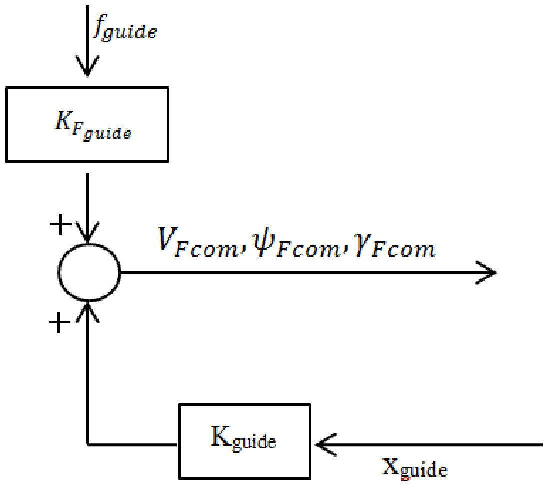

Figure 4.3: Sdre Guidance Block Diagram

$$B_{guide} = \begin{bmatrix} 0 & 0 & 0 \\ -\cos\gamma_F \cos(\psi_F - \psi_L) & 0 & 0 \\ 0 & 0 & 0 \\ -\frac{\cos\gamma_F \sin(\psi_F - \psi_L)}{2} & -\frac{V_F \sin(\psi_F - \psi_L)\cos\gamma_F}{2(\psi_F - \psi_L)} & 0 \\ -\frac{\sin\gamma_F}{2} & 0 & -\frac{V_F \sin\gamma_F}{2\gamma_F} \end{bmatrix} \tag{4.19}$$

And, the new state vector with integral states is

$$x_{guide} = \left[\int d_{long},\ d_{long},\ \int d_{lat},\ d_{lat},\ h_r - h_f \right]^T \tag{4.20}$$

Input signal is same as before:

$$u_{guide} = [V_F,\ \psi_F - \psi_L,\ \gamma_F,]^T \tag{4.21}$$

The mismatch, f_{guide} vector becomes:

$$f_{guide} = \begin{bmatrix} 0 \\ V_L cos(\gamma_L) - \dot{\psi}_L\ sin(\psi_L)\ (x_L - x_F) + \dot{\psi}_L\ cos(\psi_L)\ (y_L - y_F) \\ 0 \\ -\dot{\psi}_L\ cos(\psi_L)\ (x_L - x_F) - \dot{\psi}_L\ sin(\psi_L)\ (y_L - y_F) \\ V_L\ sin(\gamma_L) \end{bmatrix} \tag{4.22}$$

In this formulation, it is seen that the integral states of d_{long} and d_{lat} are added to the system which will help to drive the steady state errors to zero.

4.3 Simulation Results

In this part, designed controllers are tested. There are two different simulation scenarios. In Scenario-1, designed two alternative formation controllers with integral states and without integral states are tested. In this test, effect of added integral states on steady states can be compared. Scenario-2 consists of more rapid maneuvers and in this scenario, only design without integral states is used. In both scenarios, desired formation structure is given in Fig. 4.4.

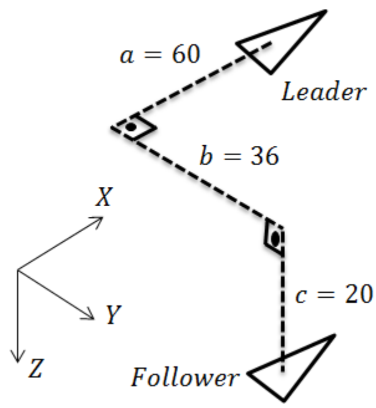

Figure 4.4: Desired Formation Structure

Scenario-1:

For the controllers and the guidance loop the weighting matrices, Q and R must be properly chosen. These weighting matrices can be constant or they can change during flight. In this study, after some trial and error, constant Q and R matrices are given below:

$$Q_{long} = diag[4 \times 10^{-4}, 4 \times 10^{-4},\ 3.65,\ 111.61] \tag{4.23}$$

$$R_{long} = diag[2 \times 10^{-2}, 1.6 \times 10^{-3}] \tag{4.24}$$

$$Q_{lat} = diag[5.6 \times 10^{-3}, 2 \times 10^{-2},\ 3.65 \times 10^{-2},\ 1.216] \tag{4.25}$$

$$R_{lat} = diag[8.3 \times 10^{-3}, 2.2 \times 10^{-3}] \tag{4.26}$$

For the guidance loop and alternative design without integral states Q_{guide} and R_{guide} are as follows:

$$Q_{guide} = diag[5 \times 10^{-2}, 1 \times 10^{-5},\ 1 \times 10^{-5}] \tag{4.27}$$

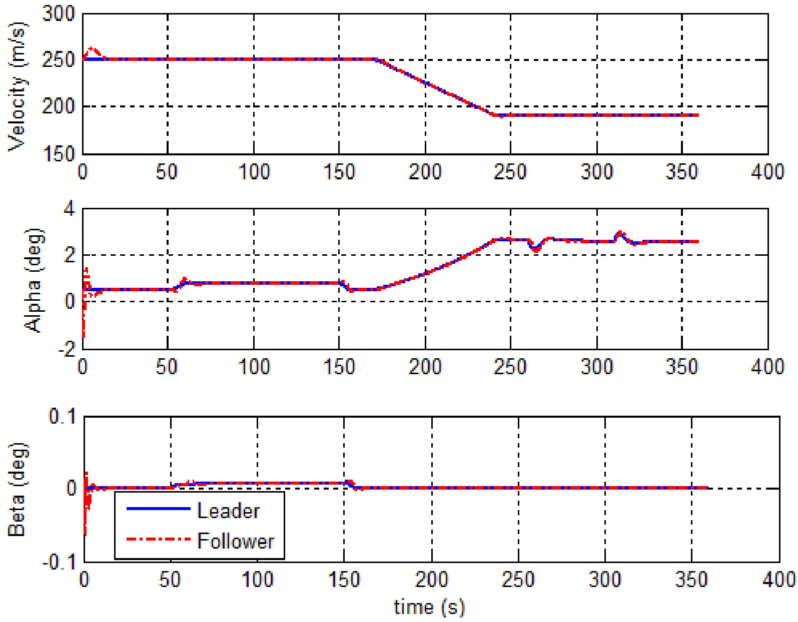

Figure 4.5: Total Speed, angle of attack, sideslip angles without using integral states in the SDRE method, Scenario-1

$$R_{guide} = diag[1, 1, 1] \tag{4.28}$$

Simulation results for the formulation without integral states are given in Fig. 4.5 - 4.11. In Fig. 4.5; speed, angle of attack and sideslip angles of leader and the follower are given. It may be observed from the figure that leader aircraft changes its speed in between 170s and 240s, and the follower follows it closely.

In Fig. 4.6, Euler Angles of leader and follower are given and it may be observed from the figure that the leader changes its heading in between 170s and 240s, and follower does the same. In Fig. 4.7, body angular rates of leader and the follower are given. In Fig. 4.8, altitudes of the leader and the follwer are given. It may also observed that the leader changes its altitude in between 260s and 310s, and follower aircraft does the same.

In Fig. 4.9 and 4.10, control surface deflections of the leader and the follower are given. It may be observed from the figure that they are realizable.

Fig. 4.11 gives the formation errors. At the beginning of the simulation follower is not on point "R" so there are formation errors in all coordinates. When the simulation starts, follower aircraft rapidly goes to the reference point "R" so formation errors

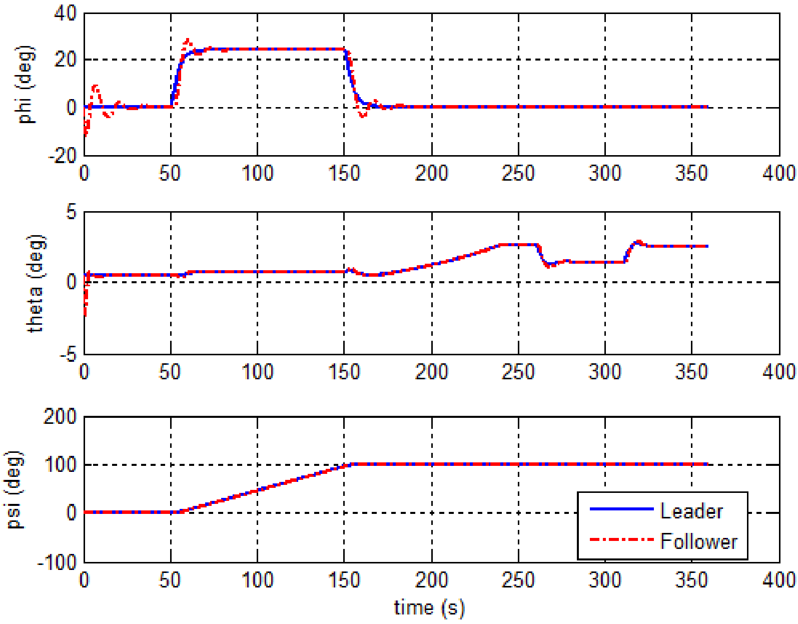

Figure 4.6: Euler Angles without using integral states in the SDRE method, Scenario-1

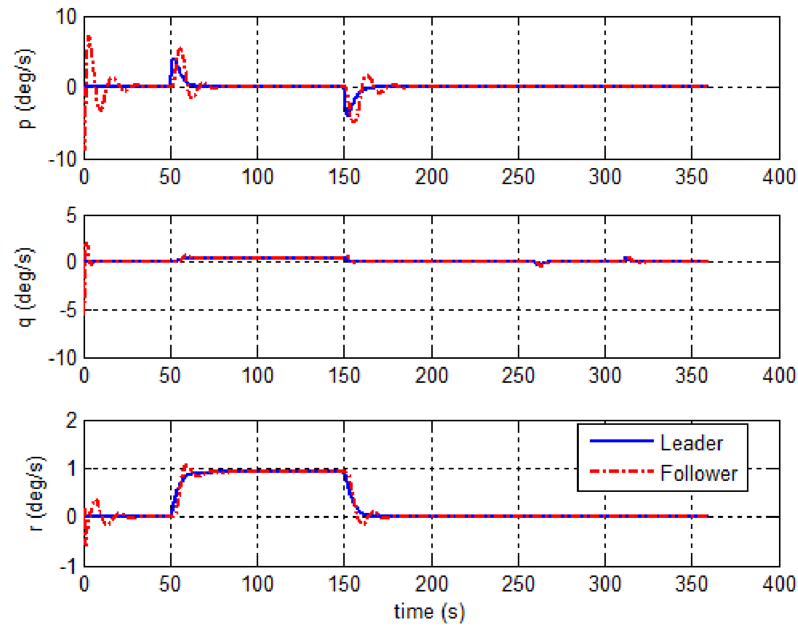

Figure 4.7: Body angular rates without using integral states in the SDRE method, Scenario-1

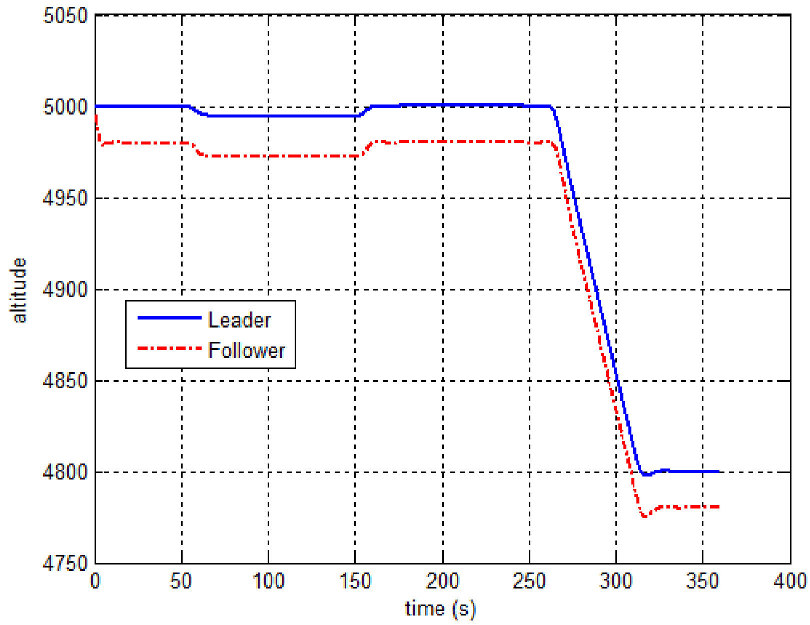

Figure 4.8: Altitude of the leader and the follower without using integral states in the SDRE method, Scenario-1

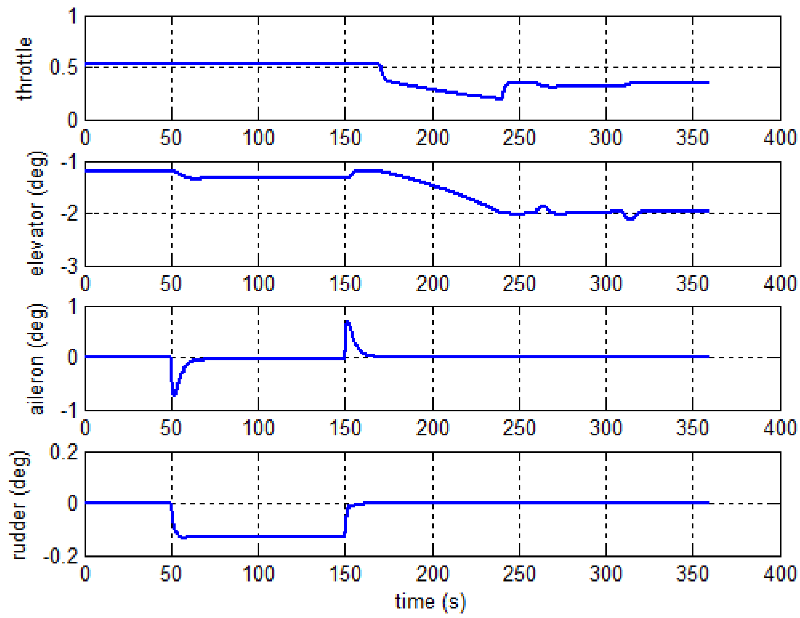

Figure 4.9: Control surface deflections of the leader without using integral states in the SDRE method, Scenario-1

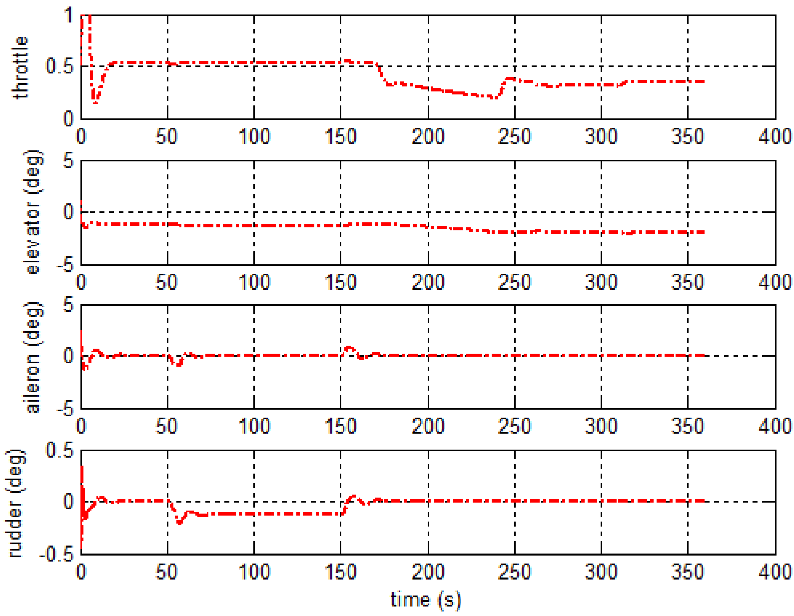

Figure 4.10: Control surface deflections of the follower without using integral states in the SDRE Method, Scenario-1

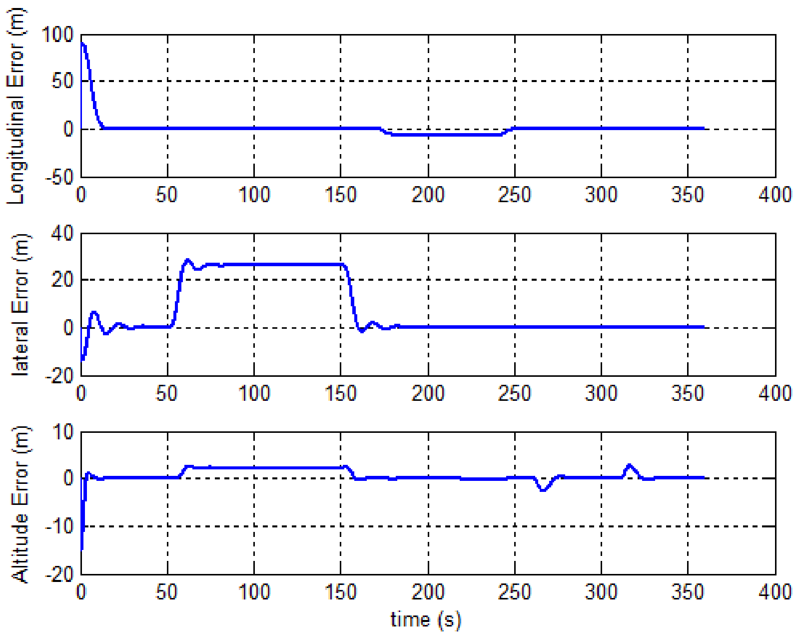

Figure 4.11: Formation errors without using integral states in the SDRE method, Scenario-1

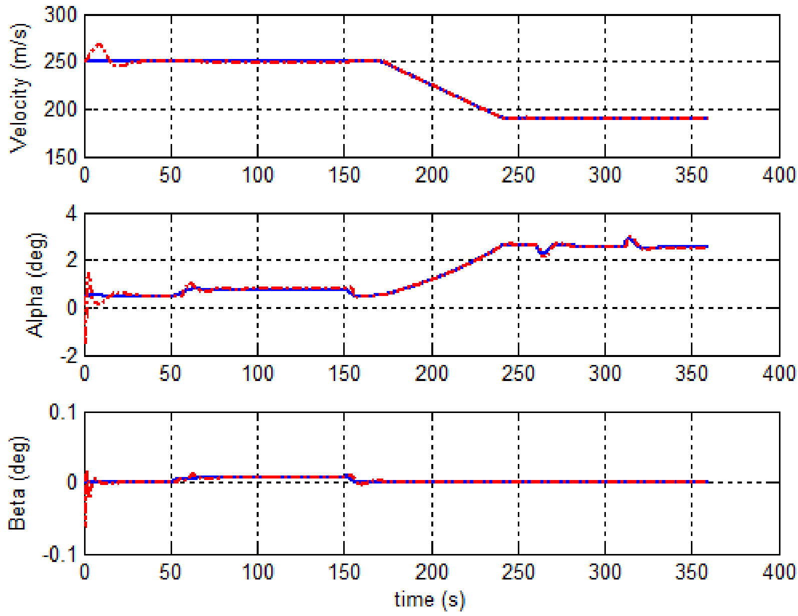

Figure 4.12: Total speed, angle of attack, sideslip angles after using integral states in the SDRE method, Scenario-1

goes to zero. In Fig. 4.11, it may be seen that lateral error is growing after 50s and after 150s it goes the zero again. Thus, there is a tracking error during the maneuver. On the other hand, between 170s and 240s, there is a tracking error at the longitudinal channel where the total speed changes. After the maneuver it also goes to zero. The relative position errors are presented in the Fig. 4.11, shows that the algorithm is quite successful. However, there are some tracking errors during the maneuver.

To reduce steady state errors, integral states are added. The weighting matrices employed are:

$$Q_{guide} = diag[5 \times 10^{-4}, 1 \times 10^{-2},\ 1 \times 10^{-7},\ 1 \times 10^{-6},\ 1 \times 10^{-5}] \qquad (4.29)$$

$$R_{guide} = diag[1, 1, 1] \qquad (4.30)$$

The results are presented in figures 4.12 to 4.18. From these figures it may be observed that the tracking errors are reduced when integral states are used. Fig. 4.18 shows that the relative position errors are much lower when integral states are included.

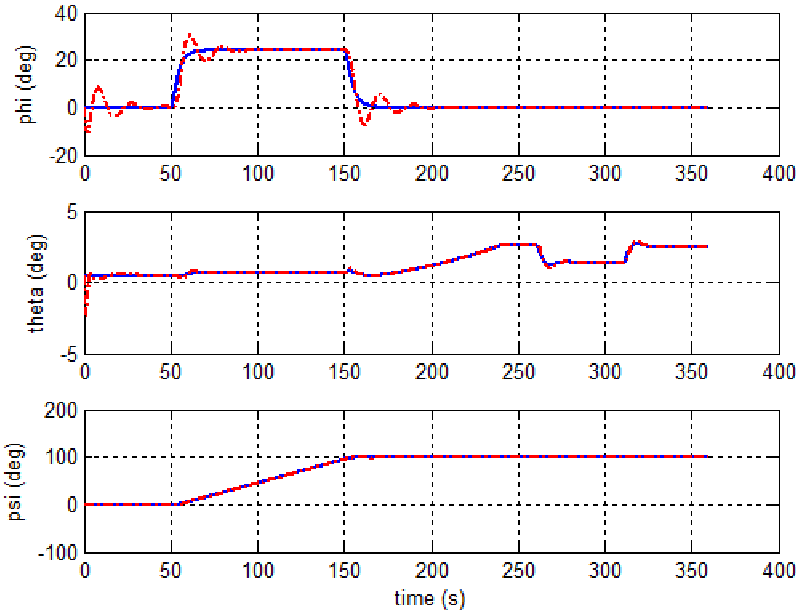

Figure 4.13: Euler Angles after using integral states in the SDRE method, Scenario-1

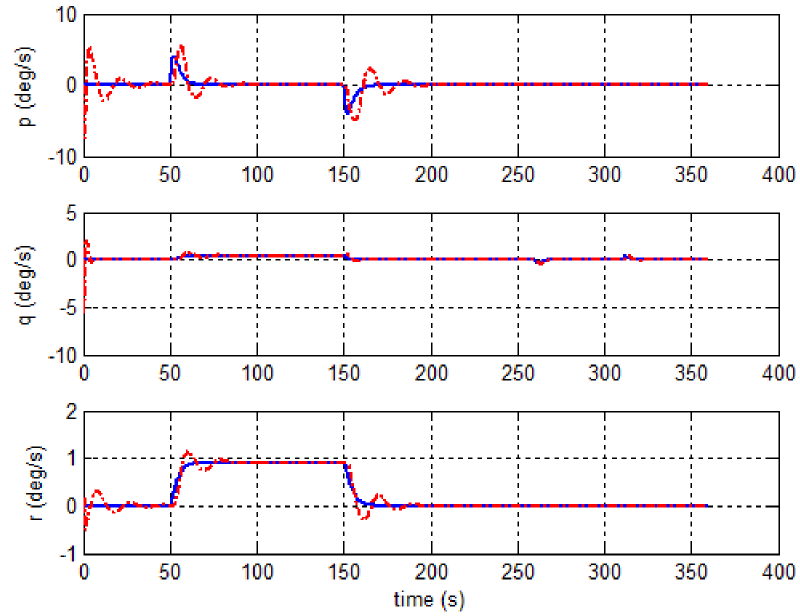

Figure 4.14: Body angular rates after using integral states in the SDRE method, Scenario-1

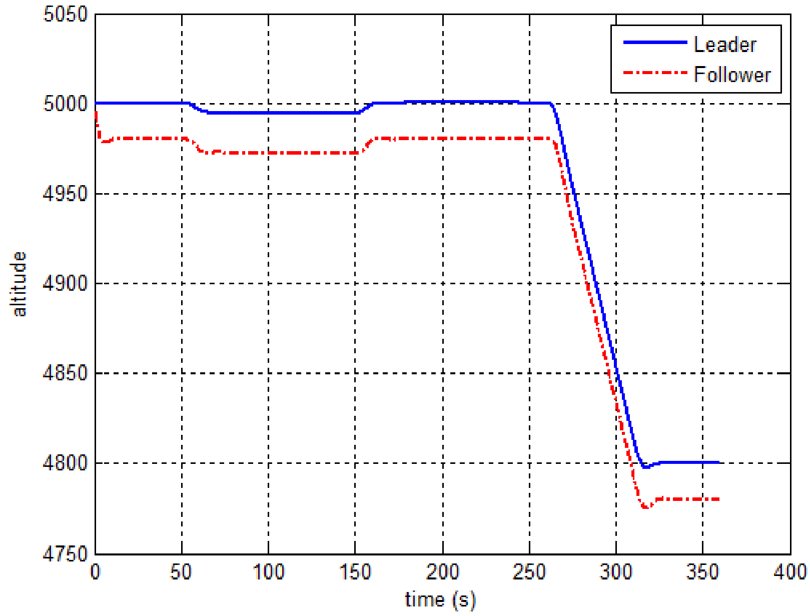

Figure 4.15: Altitude of the leader and the follower after using integral states in the SDRE method, Scenario-1

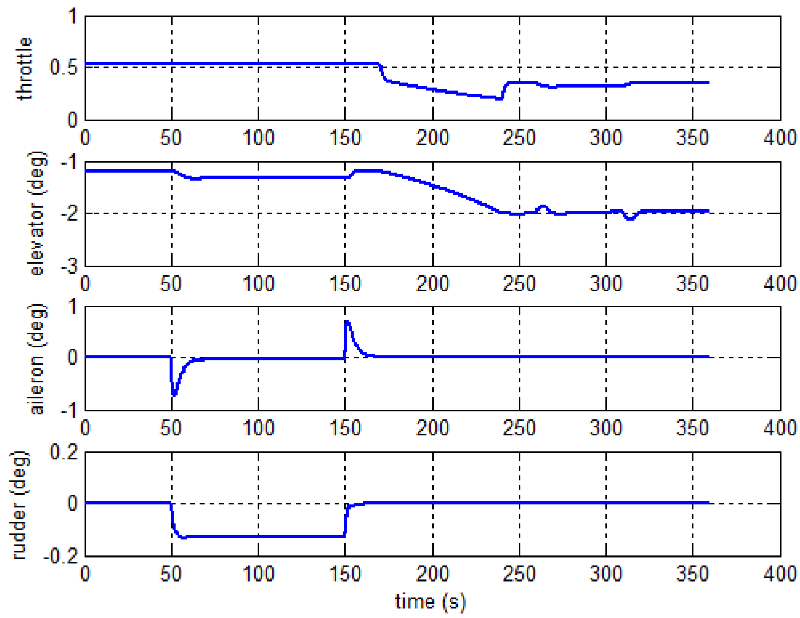

Figure 4.16: Control surface deflections of the leader after using integral states in the SDRE method, Scenario-1

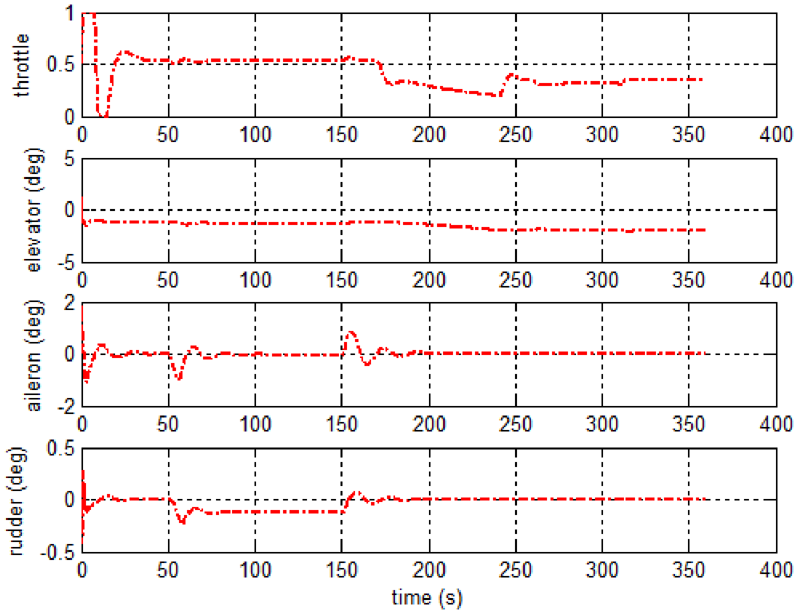

Figure 4.17: Control surface deflections of the follower after using integral states in the SDRE Method, Scenario-1

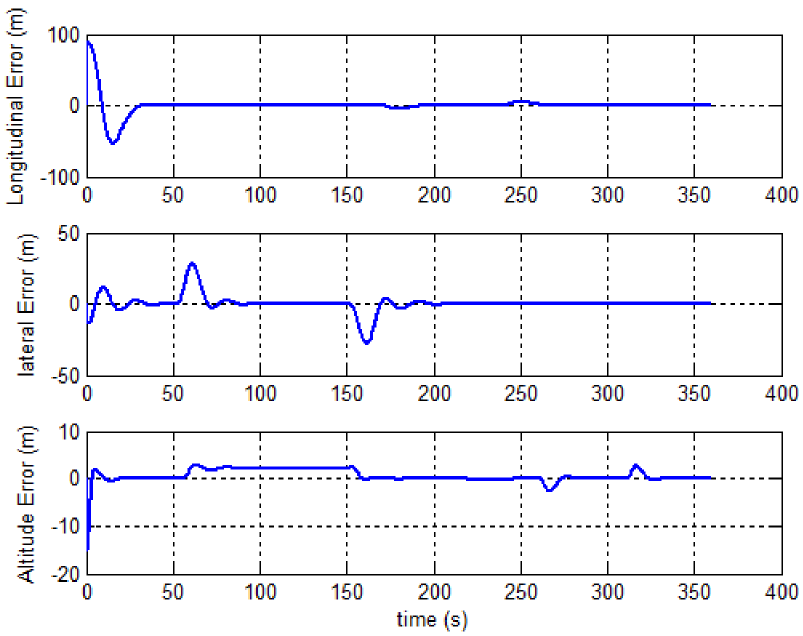

Figure 4.18: Formation errors after using integral states in the SDRE method, Scenario-1

Scenario-2:

In this scenario the leader carries out more rapid maneuver than Scenario-1. Thus, the commands to change speed, heading and altitude are much faster. In addition, flight conditions such as altitude and speed are different than Scenario-1. However, desired formation structure is same. In this scenario, SDRE guidance design without using integral states is tested to amplify the effects of rapid maneuvers. However, weighting matrices for both guidance and flight controllers are same with those used in the previous scenario.

Simulation results are presented in figures 4.19 to 4.25. In Fig. 4.19; speed, angle of attack and sideslip angles of leader and follower are given. Now, both leader and follower starts with 120 m/s and it may be observed in the figure that leader changes its speed in between 100s and 120s. It may be observed that the follower imitates the leader closely.

In Fig. 4.20, Euler angles of leader and follower are given and it is seen that in the figure leader changes its heading in between 50s and 70s, and again the follower follows quite closely.

In Fig. 4.22, altitudes of the leader and the follower are given. It is also seen that the leader changes its altitude in between 140s and 170s. Finally, formation errors are given in Fig. 4.25.

In this scenario, follower aircraft is also away from the reference point "R" at the beginning of the simulation. After the simulation starts follower goes to the point "R" and formation error goes to zero. Thus, the tracking of the follower is quite fast. On the other hand the control surface deflections and the throttle values are quite reasonable (Fig. 4.24).

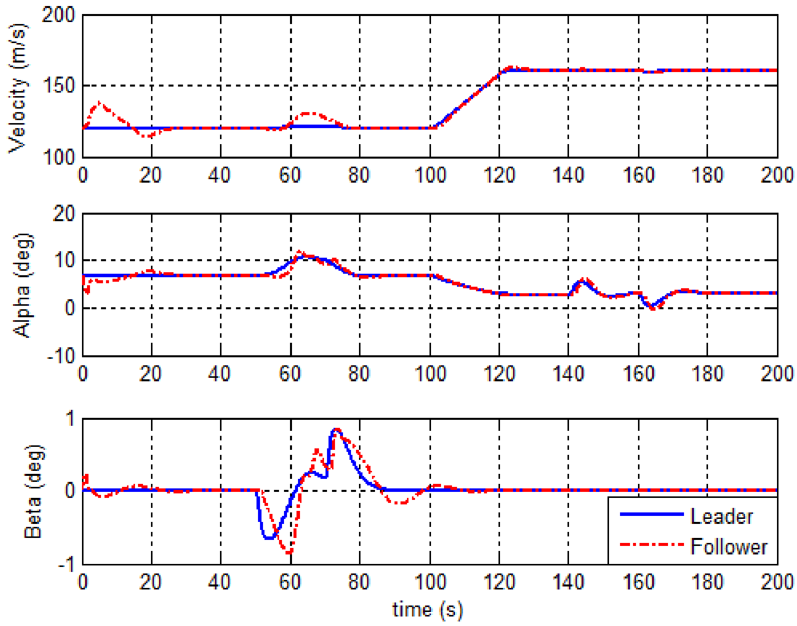

Figure 4.19: Total speed, angle of attack, sideslip angles without using integral states in the SDRE method, Scenario-2

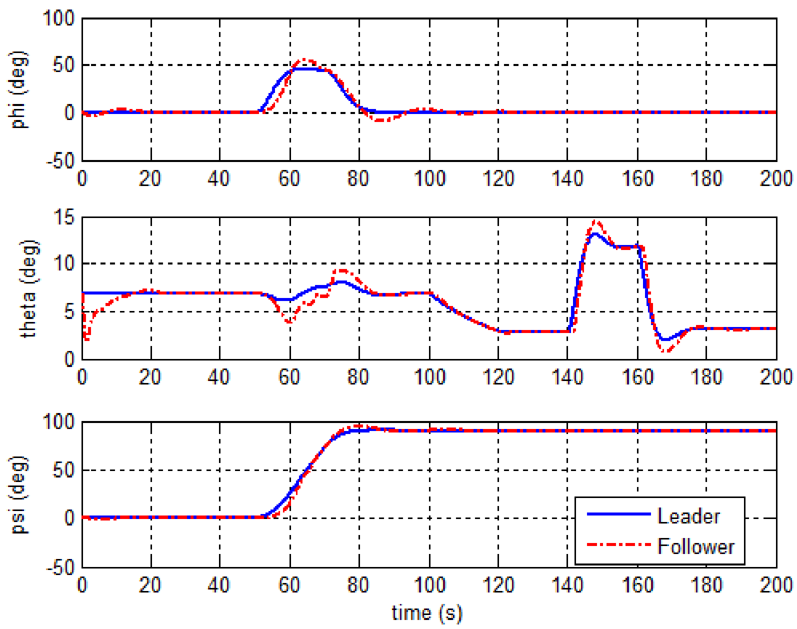

Figure 4.20: Euler Angles without using integral states in the SDRE method, Scenario-2

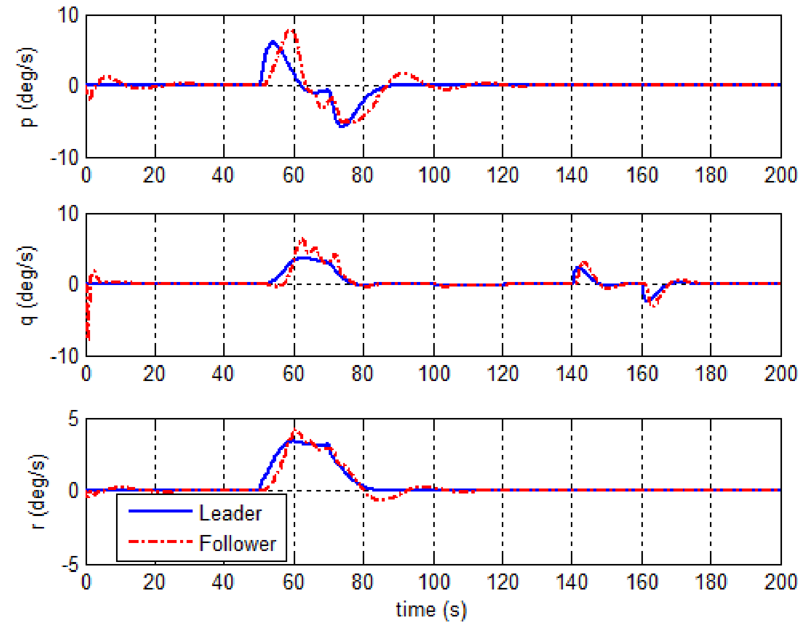

Figure 4.21: Body angular rates without using integral states in the SDRE method, Scenario-2

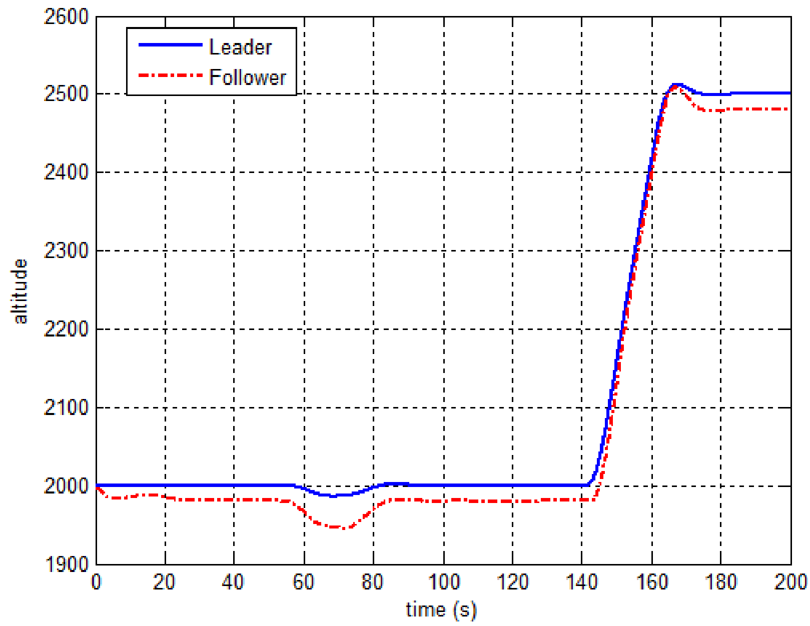

Figure 4.22: Altitude of the leader and the follower without using integral states in the SDRE method, Scenario-2

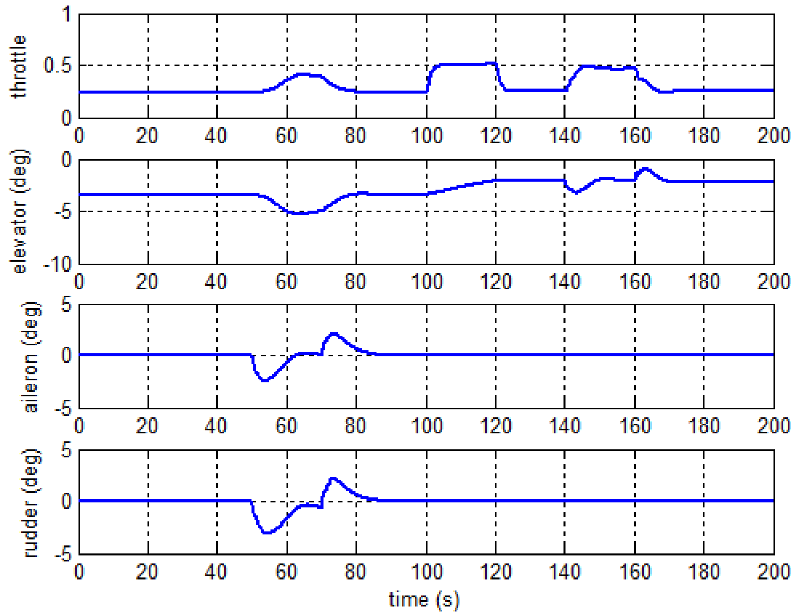

Figure 4.23: Control surface deflections of the leader without using integral states in the SDRE method, Scenario-2

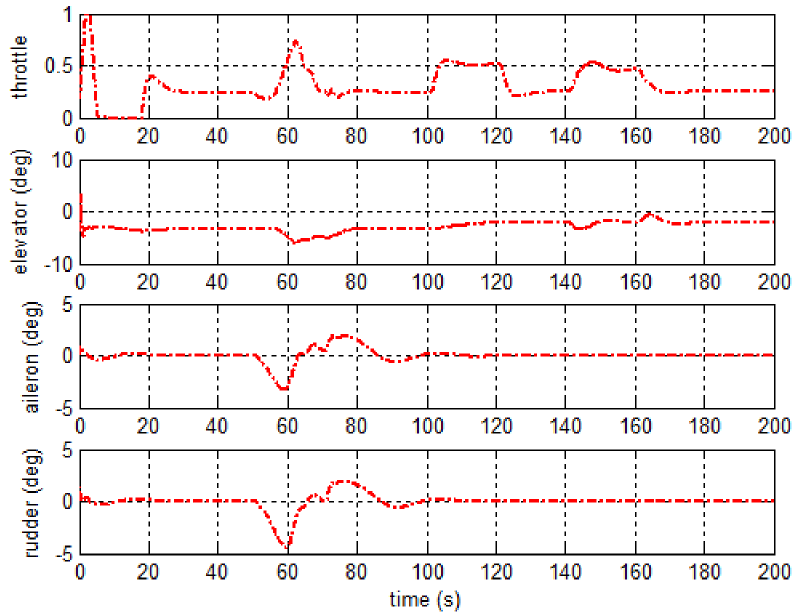

Figure 4.24: Control surface deflections of the follower without using integral states in the SDRE method, Scenario-2

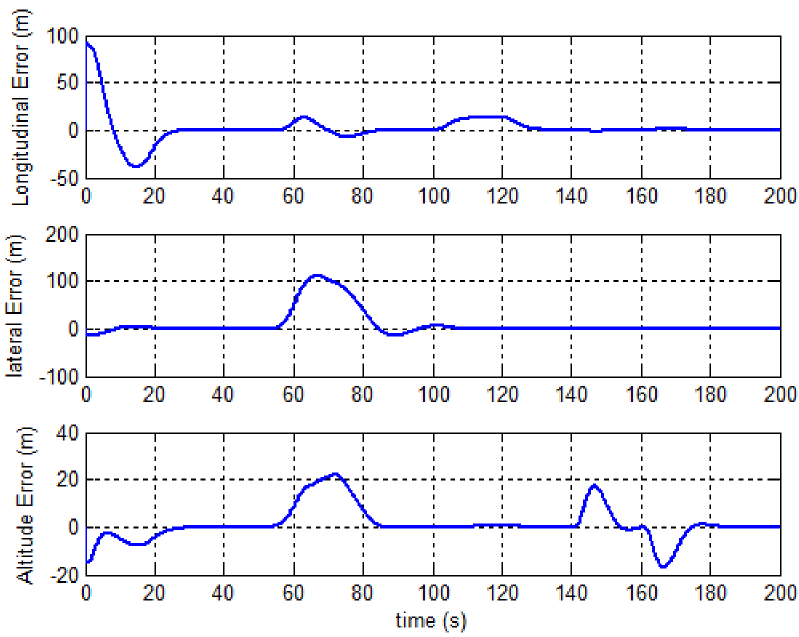

Figure 4.25: Formation errors without using integral states in the SDRE method, Scenario-2

4.4 Controllability

In this part, controllability of the proposed formation controller developed with SDRE method is investigated. For the design without integral states, proposed SDC matrices were given in Eq. 4.14 and Eq. 4.15. A matrix is zero so controllability depends on the input matrix B. If there is a singularity in the B matrix this can cause loss of controllability. The matrix B has three different parameters: $V_F, \psi_F - \psi_L, \gamma_F$. It should be checked that if any combination of these parameters leads to a zero term in the B matrix. V_F is not expected to be zero so it is not included. Flight path angle γ_F may be zero as well as $\psi_F - \psi_L$. In this case B matrix will be such that:

$$B_{guide} = \begin{bmatrix} -1 & 0 & 0 \\ 0 & \frac{-V_F}{2} & 0 \\ 0 & 0 & \frac{-V_F}{2} \end{bmatrix} \tag{4.31}$$

It is seen in the Eq. 4.31 that B matrix has still full rank. Therefore, it is controllable. A second combination may be $\gamma_F = 0$ and $\psi_F - \psi_L = \frac{\pi}{2}$. In this case B matrix is given below:

$$B_{guide} = \begin{bmatrix} 0 & 0 & 0 \\ -\frac{1}{2} & -\frac{V_F}{\pi} & 0 \\ 0 & 0 & \frac{-V_F}{2} \end{bmatrix} \tag{4.32}$$

Unfortunately, rank of the controllability matrix becomes 2 and the controllability is lost. However, in the formation flight $\psi_F - \psi_L = \frac{\pi}{2}$ case can occur for a very short time and although controllability is lost, controller can work with the previously generated gains. Therefore, $\gamma_L = 0$ and $\psi_F - \psi_L = \frac{\pi}{2}$ combination is not expected to be a major problem for this guidance algorithm. Other combinations may be $\gamma_F = \pi/2$ and $\psi_F - \psi_L = 0$; $\gamma_F = \pi/2$ and $\psi_F - \psi_L = \frac{\pi}{2}$. However, $\gamma_F = \pi/2$ is out of interest for the formation flight, it is not expected aircrafts climb straight up.

In the alternative design with integral states A and B matrices were given in Eq. 4.18 and Eq. 4.19. Same combinations are also valid in this design. Therefore, for first combination with $\gamma_F = 0$ and $\psi_F - \psi_L = 0$, B matrix is given:

$$B_{guide} = \begin{bmatrix} 0 & 0 & 0 \\ -1 & 0 & 0 \\ 0 & 0 & 0 \\ 0 & -\frac{V_F}{2} & 0 \\ 0 & 0 & -\frac{V_F}{2} \end{bmatrix} \tag{4.33}$$

For the given B matrix in Eq. 4.33, controllability matrix has full rank. Therefore, controller is controllable in this case. For second combination with $\gamma_F = 0$ and $\psi_F - \psi_L = \frac{\pi}{2}$, B matrix is given as follows:

$$B_{guide} = \begin{bmatrix} 0 & 0 & 0 \\ 0 & 0 & 0 \\ 0 & 0 & 0 \\ -\frac{1}{2} & -\frac{V_F}{\pi} & 0 \\ 0 & 0 & -\frac{V_F}{2} \end{bmatrix} \tag{4.34}$$

For the given B matrix in Eq. 4.34, controllability matrix does not have full rank so it is not controllable. However, as explained before, this case will occur in a very short time.

As a result, SDRE based formation controller can only lose its controllability in case that $\gamma_F = 0$ and $\psi_F - \psi_L = \frac{\pi}{2}$. However, $\psi_F - \psi_L = \frac{\pi}{2}$ situation will happen in a very short time. Therefore, controller can also work in these situations with previously used gain.

4.5 Comparison with LQR Based Formation Controller

In this part, SDRE based formation flight controller is compared with LQR based formation controller. First, nonlinear formation equations given in 4.7 are linearized. The trim values chosen as:

$$x_{guide} = [d_{long}, d_{lat}, h_R - h_F] = [0, 0, 0] \tag{4.35}$$

$$u_{guide} = [V_F, \psi_F - \psi_L, \gamma_F] = [250, 0, 0] \tag{4.36}$$

For these trim values, A and B matrices after linearization are:

$$A'_{guide} = \begin{bmatrix} 0 & 0 & 0 \\ 0 & 0 & 0 \\ 0 & 0 & 0 \end{bmatrix} \tag{4.37}$$

$$B'_{guide} = \begin{bmatrix} -1 & 0 & 0 \\ 0 & -250 & 0 \\ 0 & 0 & -250 \end{bmatrix} \tag{4.38}$$

And the system equation is given:

$$\dot{\tilde{x}}_{guide} = A_{guide}\tilde{x}_{guide} + B_{guide}\tilde{u}_{guide} \tag{4.39}$$

In the above equation $\tilde{x}$ and $\tilde{u}$ indicates variations from trim values. For regulator formulation, cost function is given:

$$J(x_0, u) = \frac{1}{2}\int_0^\infty \left\{x^T(t)Qx(t) + u^T(t)Ru(t)\right\} dt \tag{4.40}$$

First, weight matrices Q and R chosen as below:

$$Q = diag[5e-2, 1e-5, 1e-5] \tag{4.41}$$

$$R = diag[1, 1, 1] \tag{4.42}$$

Then the feedback gain matrix becomes,

$$K = diag[0.2236, 0.0032, 0.0032] \tag{4.43}$$

For the chosen weight, first simulation test case is named as case-1. To test the controller, simulation Scenario-1 is used and the results are given in Fig. 4.26.

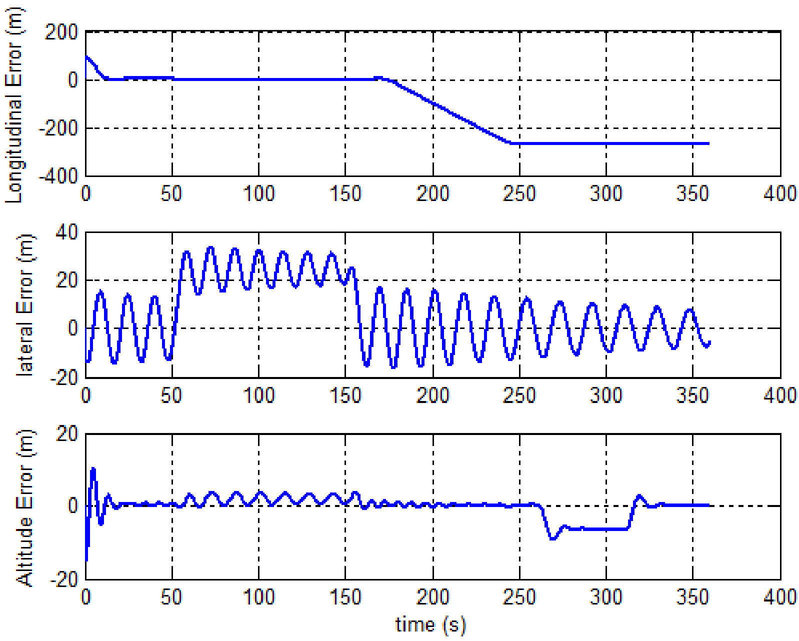

Figure 4.26: Formation errors with LQR method, case-1

From figure 4.26 it may be observed that the lateral response is oscillatory. For that reason, weight of d_{lat} is reduced and weight matrices are chosen as below:

$$Q = diag[5e-2, 1e-6, 1e-5] \tag{4.44}$$

$$R = diag[1, 1, 1] \tag{4.45}$$

Then the feedback gain matrix becomes:

$$K = diag[0.2236, 1e-3, 0.0032] \tag{4.46}$$

This case is named as case-2 and results are given in Fig. 4.27. According to the Fig. 4.27, oscillatory motion does not exist any more. However, the longitudinal error is large so in test case-3 weight of d_{long} is increased and new weight matrices are given:

$$Q = diag[1e-1, 1e-6, 1e-5] \tag{4.47}$$

$$R = diag[1, 1, 1] \tag{4.48}$$

The feedback gain matrix becomes:

$$K = diag[0.3162, 1e-3, 0.0032] \tag{4.49}$$

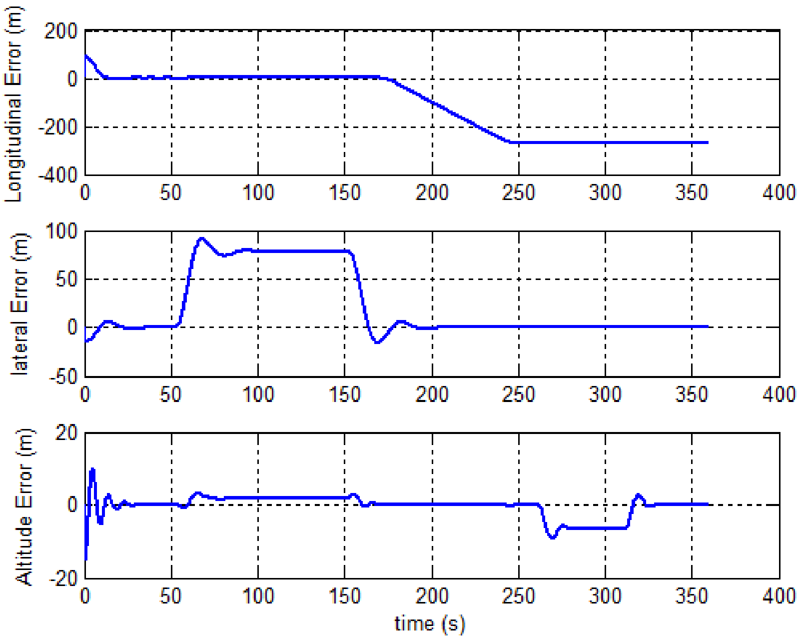

Figure 4.27: Formation Errors with LQR method, case-2

Results are given in Fig. 4.28. With increased weight, longitudinal error is reduced but it is not enough so weight is increased once more in test case-4. For the test case-4 weights are given below:

$$Q = diag[0.5, 1e-6, 1e-5] \tag{4.50}$$

$$R = diag[1, 1, 1] \tag{4.51}$$

The feedback gain matrix becomes:

$$K = diag[0.7071, 1e-3, 0.0032] \tag{4.52}$$

And the results are given in Fig. 4.29. The figure shows that increased weights help to reduce longitudinal error more but at the beginning of the simulation, oscillatory motion is present.

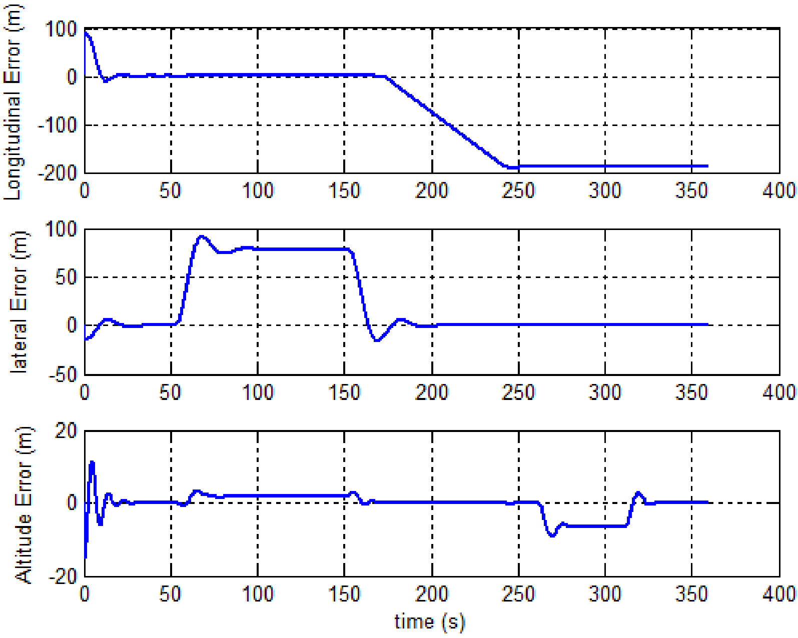

Figure 4.28: Formation errors with LQR method, case-3

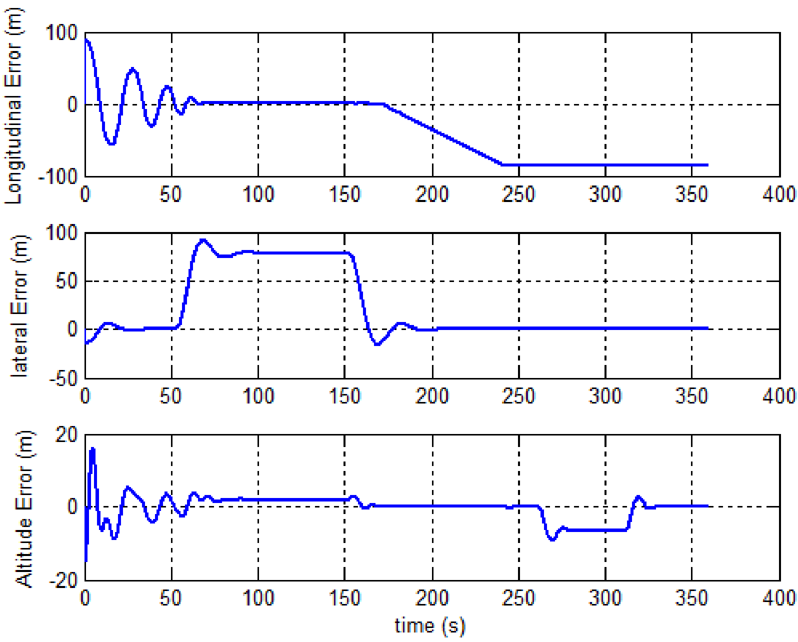

Figure 4.29: Formation errors with LQR method, case-4

Last test is conducted with increased d_{long} weight again. One more time, chosen weights are given:

$$Q = diag[0.8, 1e-6, 1e-5] \tag{4.53}$$

$$R = diag[1, 1, 1] \tag{4.54}$$

The feedback gain matrix becomes:

$$K = diag[0.8944, 1e-3, 0.0032] \tag{4.55}$$

And the results are given in Fig. 4.30. The figure shows that oscillatory motion is increasing with d_{long} weight however to reduce the error it should be increased. Therefore, it leads to a conflict. To solve this problem, gain scheduling method could be used or weight matrices can change with time. On the other hand, SDRE based method was solving this problem without using gain scheduling or another method. For different maneuvers it could be hard to design these gains. Thus, SDRE based method is better than LQR.

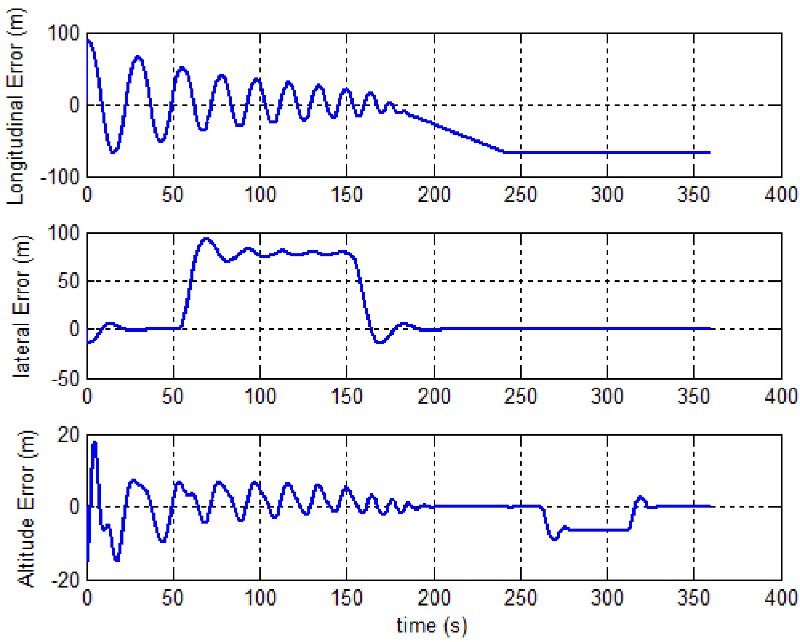

Figure 4.30: Formation errors with LQR method, case-5

CHAPTER 5

LYAPUNOV FUNCTION BASED FORMATION CONTROL

5.1 Formation Control Design

In this section, Lyapunov function is used to formulate a guidance algorithm. Formation kinematics and equations derived previously are used.

The goal of the guidance is to bring the distances from the follower to the desired reference point to zero. Thus, a positive definite Lyapunov function made of the squares of the distances may be used. To alleviate the steady sate error problems, the integral of longitudinal and lateral distances may also be included. Thus, the following Lyapunov function is proposed:

$$V = \frac{1}{2}\left\{d_{long}^2 + d_{lat}^2 + (h_R - h_F)^2 + (g_{11}\int d_{long})^2 + (g_{22}\int d_{lat})^2\right\} \tag{5.1}$$

Note that in the above function we did not use any scaling for position errors but added weight for the integral states. The derivative of the Lyapunov function may be written as,

$$\dot{V} = d_{long}\,\dot{d}_{long} + d_{lat}\,\dot{d}_{lat} + (h_R - h_F)\,(\dot{h}_R - \dot{h}_F) + g_{11}\,d_{long}\int d_{long} + g_{22}\,d_{lat}\int d_{lat} \tag{5.2}$$

Equating the derivative to negative definite Lyapunov function where, D_{guide} is a positive definite matrix,

$$\dot{V} = -\left[\begin{array}{c} d_{long}, d_{lat}, h_R - h_F \end{array}\right] D_{guide} \left[\begin{array}{c} d_{long} \\ d_{lat} \\ h_R - h_F \end{array}\right] \tag{5.3}$$

the following is obtained.

$$\begin{bmatrix} \dot{d}_{long} + g_{11} \int d_{long} \\ \dot{d}_{lat} + g_{22} \int d_{lat} \\ \dot{h}_R - \dot{h}_F \end{bmatrix} = -D_{guide} \begin{bmatrix} d_{long} \\ d_{lat} \\ h_R - h_F \end{bmatrix} \tag{5.4}$$

Arranging the terms, the derivatives of the distances may be written as,

$$\begin{bmatrix} \dot{d}_{long} \\ \dot{d}_{lat} \\ \dot{h}_R - \dot{h}_F \end{bmatrix} = -D_{guide} \begin{bmatrix} d_{long} \\ d_{lat} \\ h_R - h_F \end{bmatrix} - G \begin{bmatrix} \int d_{long} \\ \int d_{lat} \\ 0 \end{bmatrix} \tag{5.5}$$

where,

$$D_{guide} = diag[q_{11},\ q_{22},\ q_{33}] \tag{5.6}$$

$$G = diag[g_{11},\ g_{22},\ g_{33}] \tag{5.7}$$

Substituting $\dot{d}_{long}, \dot{d}_{lat}$ and $\dot{h}_R - \dot{h}_F$ in Eq. (4.7) into Eq. (5.5) one obtains,

$$\begin{aligned} V_F\ \cos\gamma_F\ \cos(\psi_F - \psi_L) = V_L\ \cos\gamma_L - \dot{\psi}_L\ sin\psi_L\ (X_L - X_F) \\ + \dot{\psi}_L\ cos\psi_L\ (Y_L - Y_F) + q_{11}\ d_{long} + g_{11} \int d_{long} \end{aligned} \tag{5.8}$$

$$\begin{aligned} V_F\ \cos\gamma_F\ \sin(\psi_F - \psi_L) = -\dot{\psi}_L\ cos\psi_L\ (X_L - X_F) \\ - \dot{\psi}_L\ sin\psi_L\ (Y_L - Y_F) + q_{22}\ d_{lat} + g_{22} \int d_{lat} \end{aligned} \tag{5.9}$$

$$V_F\ \sin\gamma_F = V_L\ sin\gamma_L + q_{33}\ (h_R - h_F) \tag{5.10}$$

After some simplifications, the following equations for the follower's heading, flight path angle and velocity are obtained.

$$\begin{aligned} \psi_F = atan\left(\frac{-\dot{\psi}_L \cos\psi_L (X_L - X_F) - \dot{\psi}_L \sin\psi_L (Y_L - Y_F) + q_{22} d_{lat} + g_{22} \int d_{lat}}{V_L \cos\gamma_L - \dot{\psi}_L \sin\psi_L (X_L - X_F) + \dot{\psi}_L \cos\psi_L (Y_L - Y_F) + q_{11} d_{long} + g_{11} \int d_{long}} \right) \\ + \psi_L \end{aligned} \tag{5.11}$$

$$\gamma_F = atan\left(\frac{\{V_L \sin\gamma_L + Q_{33}(h_R - h_F)\}\, cos(\psi_F - \psi_L)}{V_L \cos\gamma_L - \dot{\psi}_L \sin\psi_L(X_L - X_F) + \dot{\psi}_L \cos\psi_L(Y_L - Y_F) + q_{11}d_{long} + g_{11}\int d_{long}}\right) \tag{5.12}$$

$$V_F = \frac{V_L \cos\gamma_L - \dot{\psi}_L \sin\psi_L(X_L - X_F) + \dot{\psi}_L \cos\psi_L(Y_L - Y_F) + q_{11}d_{long} + g_{11}\int d_{long}}{\cos\gamma_F \cos(\psi_F - \psi_L)} \tag{5.13}$$

These generated ψ_F, γ_F, and V_F, are send to the follower's inner loop to realize the commands. Again, follower's inner loop works with SDRE based flight controller as before.

5.2 Simulation Results

Proposed Lyapunov function based formation control method is tested in using the same simulation scenarios presented in the previous section.

Scenario-1:

Desired formation structure was given in Fig. 4.4 and it is also used here. Weighting matrices D_{guide} and G are chosen as:

$$D_{guide} = diag[0.3,\ 0.2,\ 0.3] \tag{5.14}$$

$$G = diag[0.007,\ 0.015,\ 0] \tag{5.15}$$

The simulation results are presented in figures 5.1 to 5.7. From these results, it may be observed that although there are some oscillations in follower states, the follower follows the commands closely. In Fig. 5.5 and 5.6 control surface deflections of the leader and the follower are given. In both cases the commands are realizable for the leader and the follower. In particular the follower's throttle command saturates for a short duration. The formation errors decay rapidly and tracking is good (5.7). Thus, it may concluded that the proposed formation control method using the Lyapunov function is quite successful.

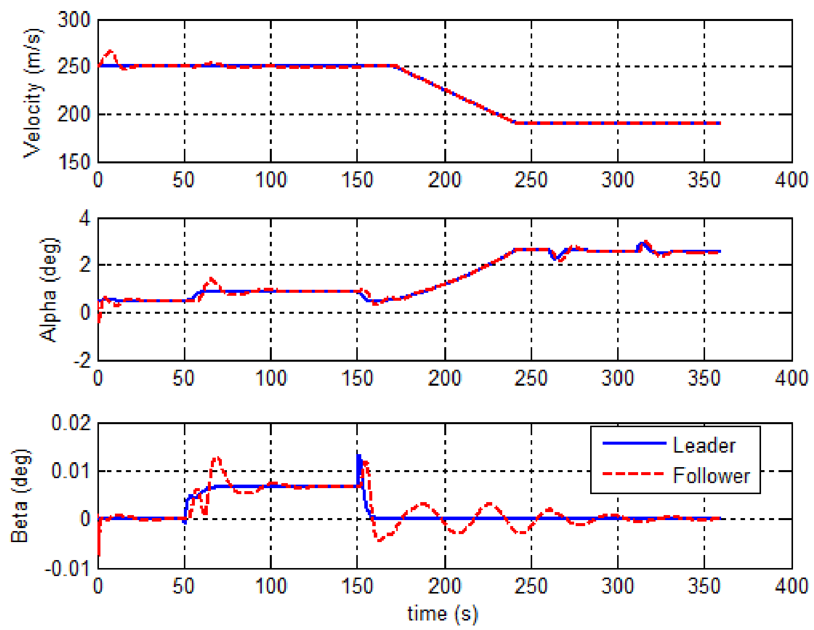

Figure 5.1: Total speed, angle of attack, sideslip angles for the Lyapunov Function method, Scenario-1

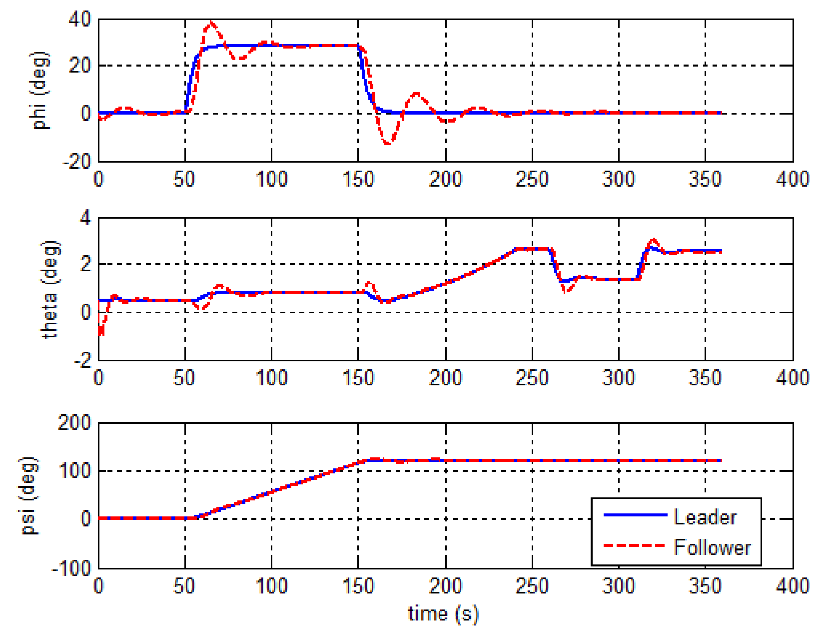

Figure 5.2: Euler Angles for the Lyapunov Function method, Scenario-1

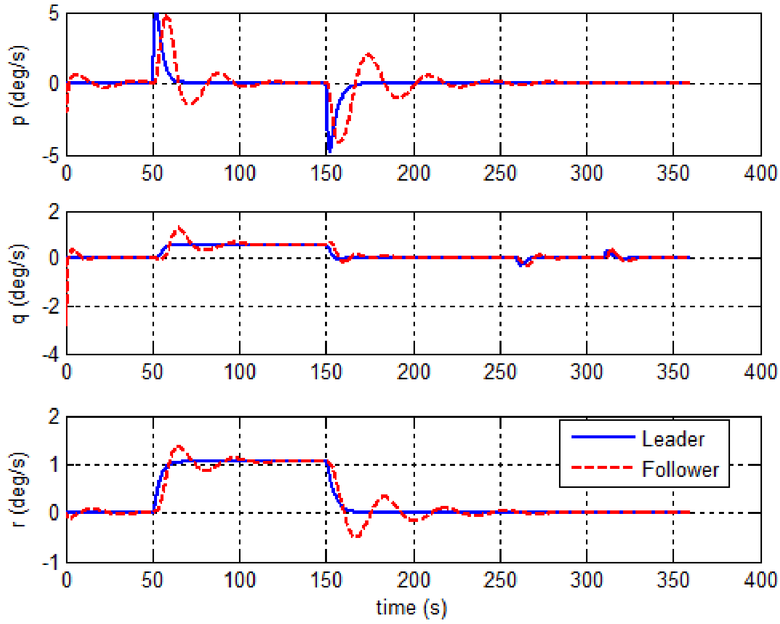

Figure 5.3: Body angular rates for the Lyapunov Function method, Scenario-1

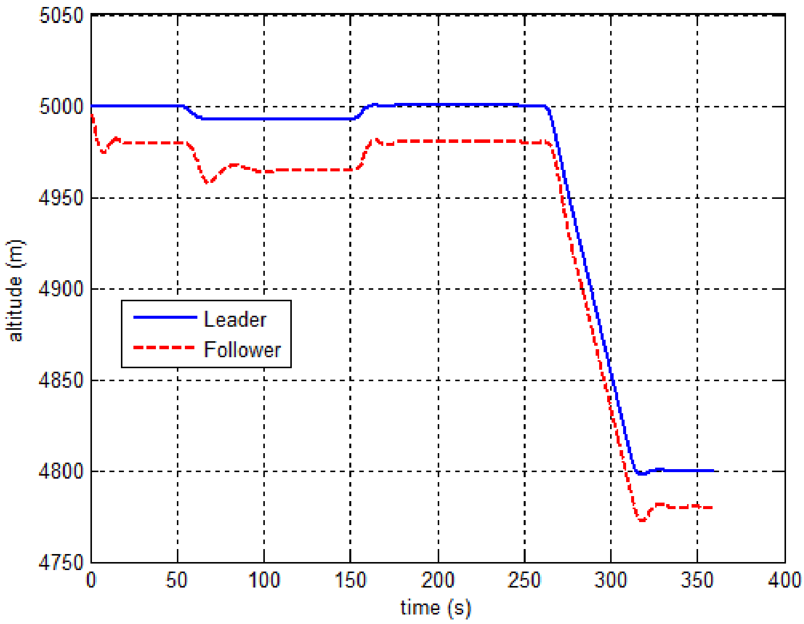

Figure 5.4: Altitude of the leader and the follower for the Lyapunov Function method, Scenario-1

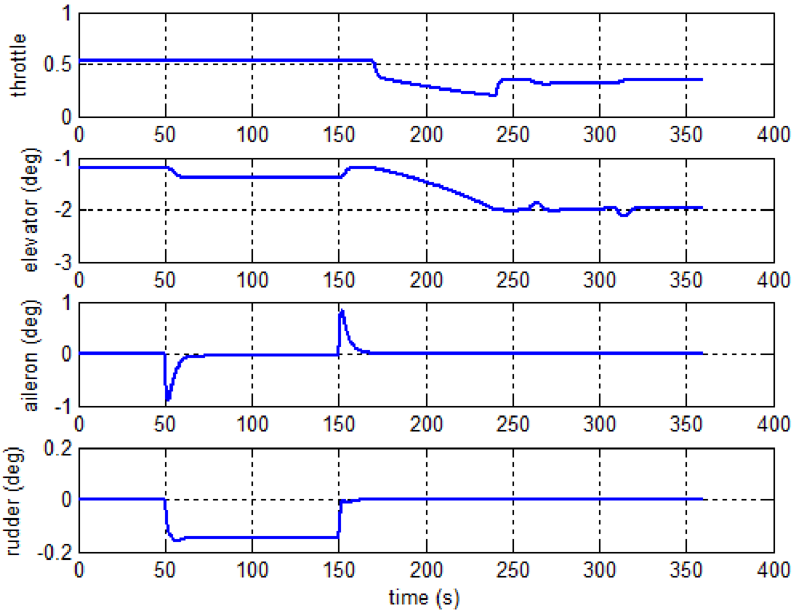

Figure 5.5: Control surface deflections of the leader for the Lyapunov Function method, Scenario-1

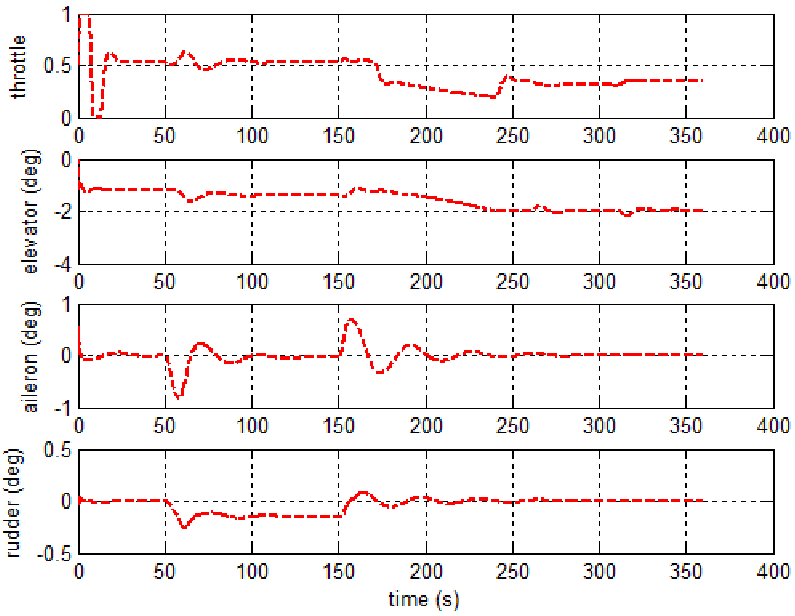

Figure 5.6: Control surface deflections of the follower for the Lyapunov Function method, Scenario-1

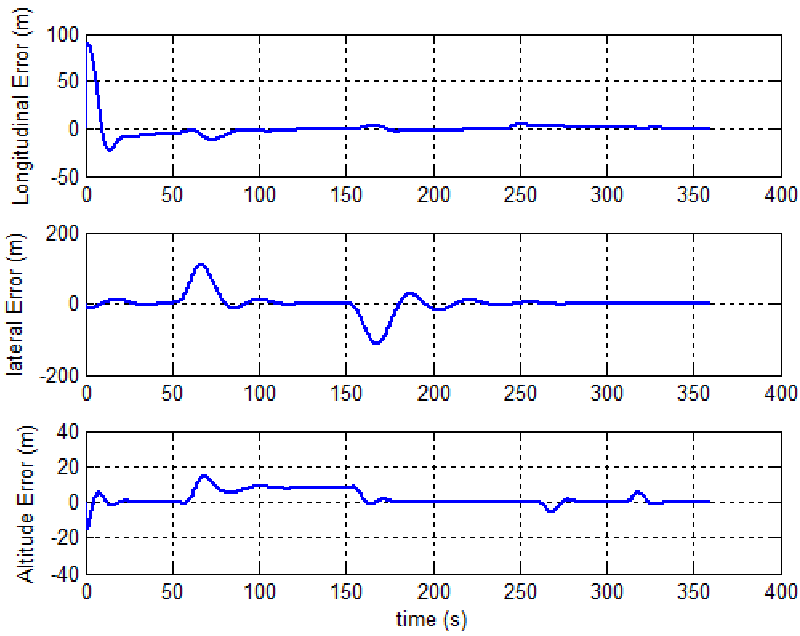

Figure 5.7: Formation errors of the follower for the Lyapunov Function method, Scenario-1

Scenario-2:

Scenario-2 has more rapid maneuvers and it is same used in previous section. Lyapunov funciton approach is also tested against this scenario, but some modifications are done in the weight matrices. These new weights are given below:

$$D_{guide} = diag[0.2,\ 0.2,\ 0.25] \tag{5.16}$$

$$G = diag[0,\ 0,\ 0] \tag{5.17}$$

One important observation is given that in SDRE method there was no need to update the weight matrices between the two different simulations. However, in Lyapunov Function method that was necessary to modify it to get better results. The simulation results are presented in figures 5.8 to 5.14.

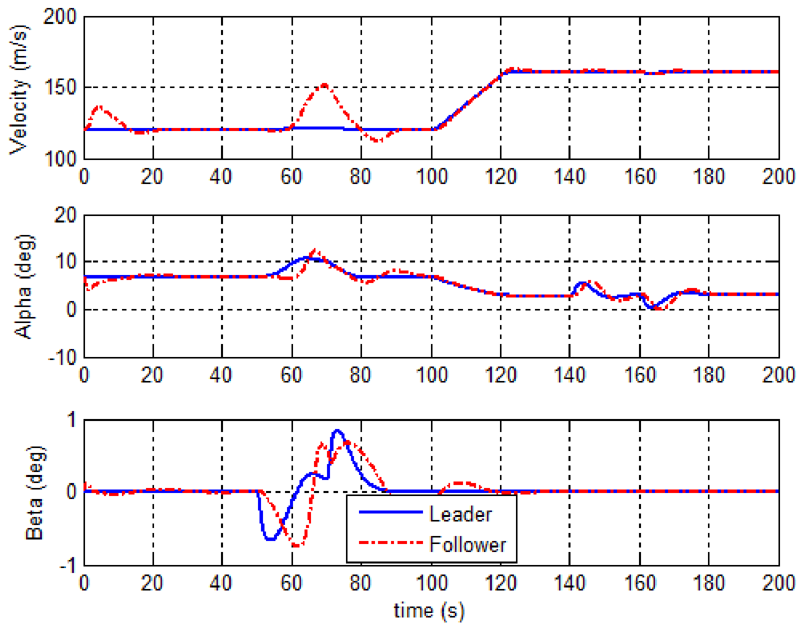

Figure 5.8: Total speed, angle of attack, sideslip angles for the Lyapunov Function method, Scenario-2

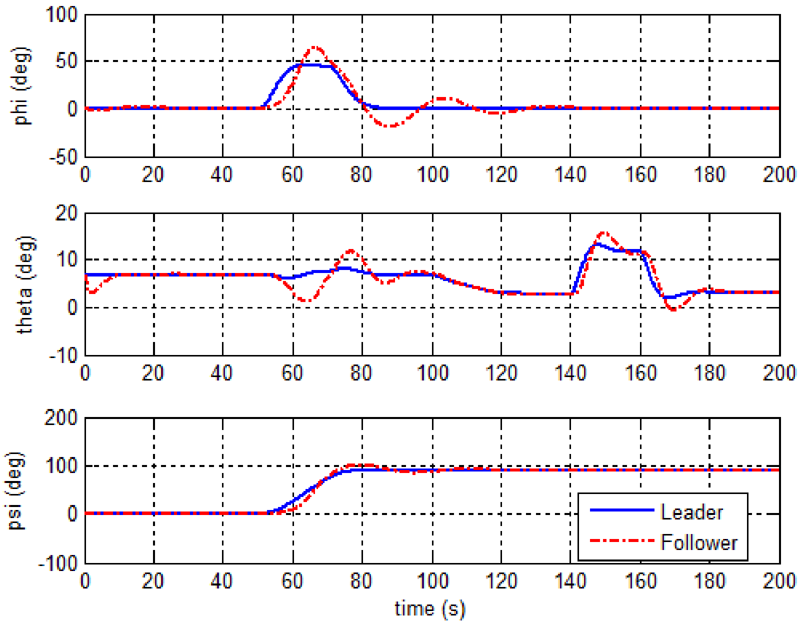

Figure 5.9: Euler Angles for the Lyapunov Function method, Scenario-2

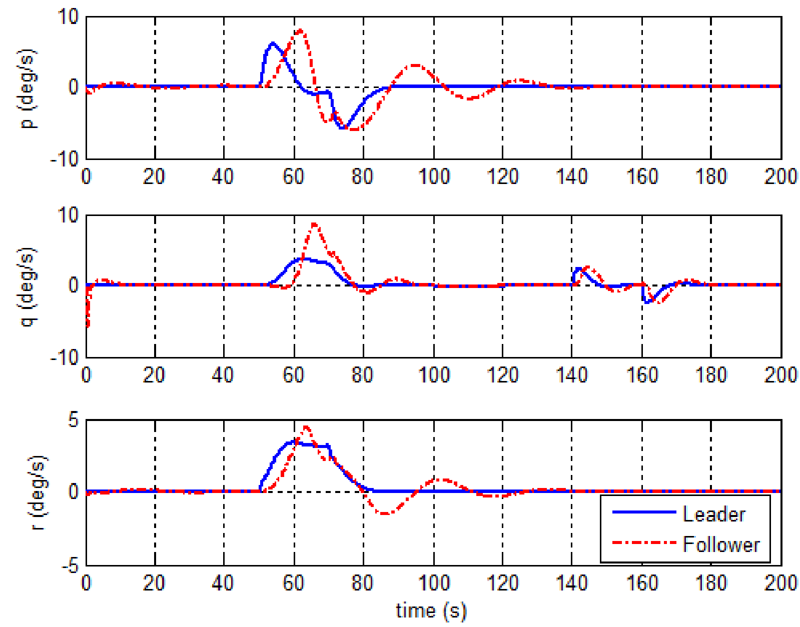

Figure 5.10: Body angular rates for the Lyapunov Function method, Scenario-2

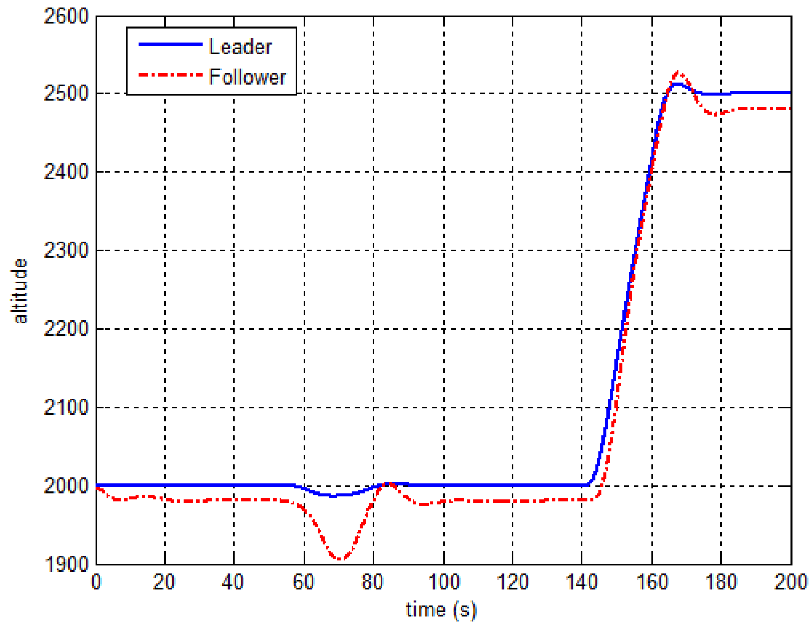

Figure 5.11: Altitude of the leader and the follower for the Lyapunov Function method, Scenario-2

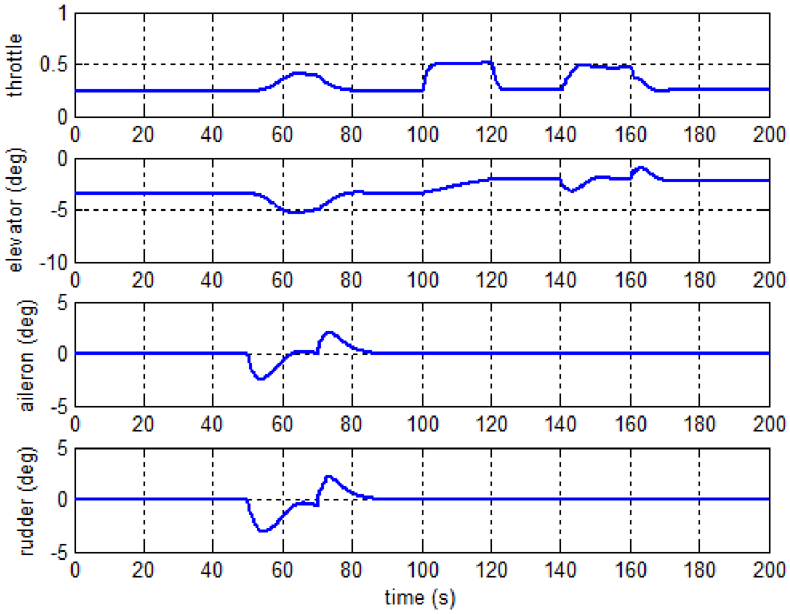

Figure 5.12: Control surface deflections of the leader for the Lyapunov Function method, Scenario-2

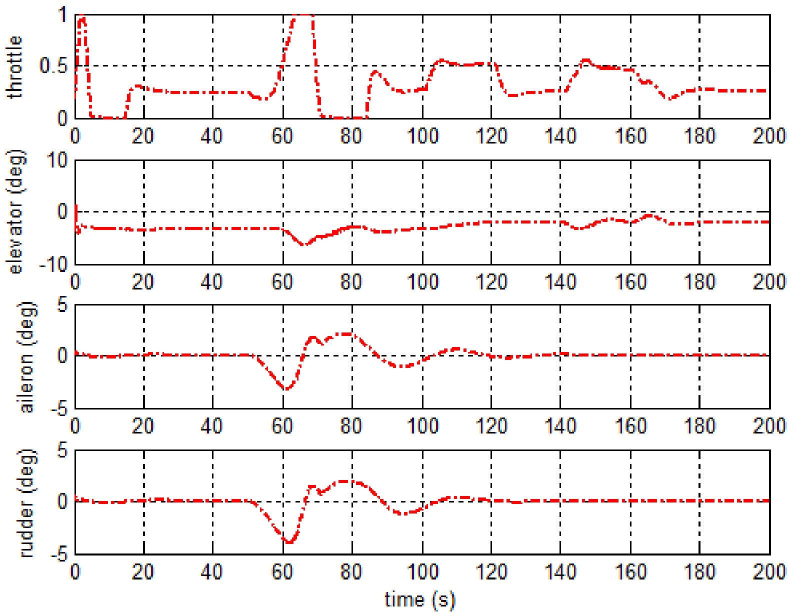

Figure 5.13: Control surface deflections of the follower for the Lyapunov Function method, Scenario-2

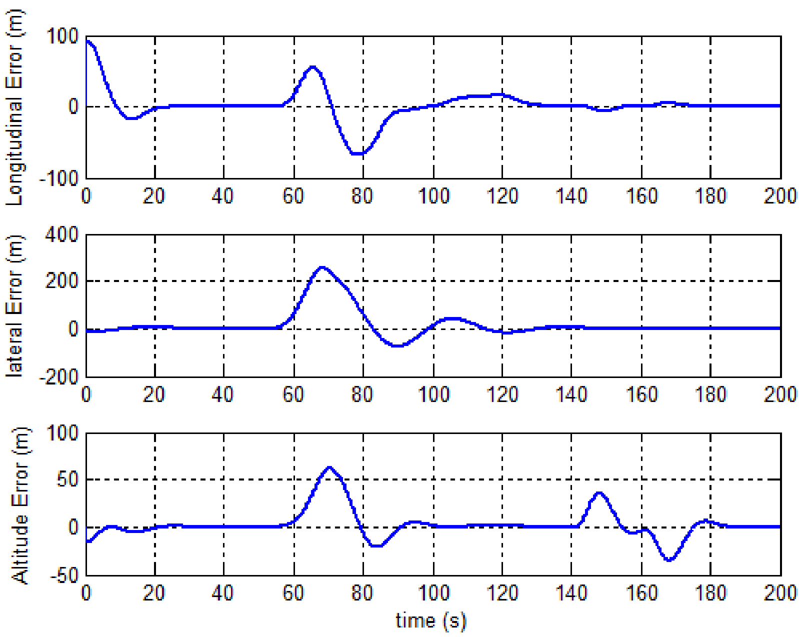

Figure 5.14: Formation errors of the follower for the Lyapunov Function method, Scenario-2

From these figures, it may be observed that the follower follows the leader quite closely. There are some tracking errors at the maneuver times (Fig. 5.14). However, these errors go to zero rapidly. It should be noted that the weighting matrices are modified from scenario-1 to scenario-2. This may indicate that adaptive weighting may be used in the guidance calculations.

5.3 Controllability

In this part, controllability of the proposed formation flight controller with Lyapunov method is investigated. In Eq. 5.11, 5.12 and 5.13, outputs of the controller were given. If there are singularities in these equations, this could lead a controllability problem. In Eq. 5.11 and 5.12, there is not a singularity problem because even if denominator of the equations are zero, atan will be resulted as $\pi/2$. On the other hand, In Eq. 5.13, denominator has $cos(\gamma_F)$ and $cos(\gamma_{\psi_F - \psi_L})$ terms and if these terms go to zero, there will be a controllability problem. Therefore, critical point is $\gamma_F = \pi/2$ or $\psi_F - \psi_L = \pi/2$. In formation flight, $\gamma_F = \pi/2$ is not expected so it is out of interest. However, $\psi_F - \psi_L = \pi/2$ can be a problem but this condition may be seen in an agile maneuver and it will be stay very short time. Therefore, various methods can be applied to remove this problem easily.

CHAPTER 6

SENSITIVITY ANALYSIS

In this chapter, sensitivity of the proposed formation flight controllers developed with SDRE and Lyapunov methods is investigated against measurement errors. SDRE and Lyapunov based formation controllers take leader's speed, heading, heading rate, flight path angle and positions. Therefore, if there is an error in these parameters what would be the effect on the formation flight is investigated in this section. These investigation is carried out using Scenario-1. On the other hand, for the SDRE based method there were two different design. In sensitivity analysis, design with integral states is used.

6.1 Error in the Speed of the Leader

In this section, speed of the leader aircraft is given to the follower with +20 m/s bias. SDRE based formation control algorithm results on relative position errors are given in Fig. 6.1. The figure shows that the follower is brought the desired relative position in spite of the error of the observed speed of the leader. There is an overshoot and some oscillations at the beginning when the position error is large. However, the follower's overall performance is acceptable.

Same scenario is used for the Lyapunov based formation controller as well and the results are given in Fig. 6.2. Similar to the SDRE controller, there is an overshoot initially but the follower aircraft is converges and tracks the desired relative position as well as the case where there is no observation error on the speed. According to the results it may be stated that both SDRE and Lyapunov based formation controllers

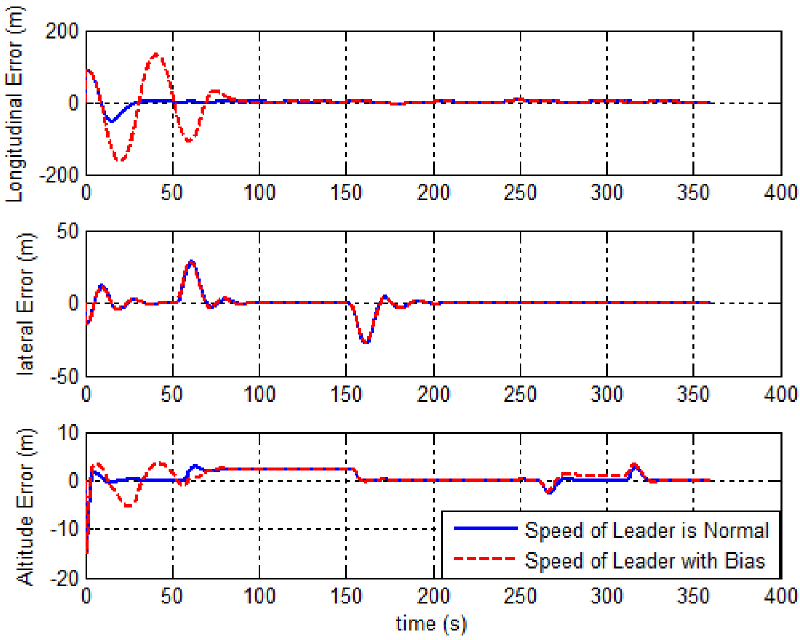

Figure 6.1: Formation results for the case that +20 m/s error in leader's speed with the SDRE method

overcome speed observation errors.

6.2 Error in the Flight Path Angle of the Leader

In this section, flight path angle of the leader is communicated to the follower aircraft with +2 degree bias. This case is first tested for the SDRE method and the results are given in Fig. 6.3. Results show that when flight path angle of the leader is given to the follower aircraft, follower can track the leader but there is an offset in the altitude channel. However, there is no tracking error in the horizontal channels since there are integral states in these channels. This offset could be made zero if integrators are added to the altitude channel as well.

Similar behaviour is observed with Lyapunov based controller (Fig. 6.4). Again, results show that while there is not error in the horizontal channels, error in the altitude channel is observable due to same reasons.

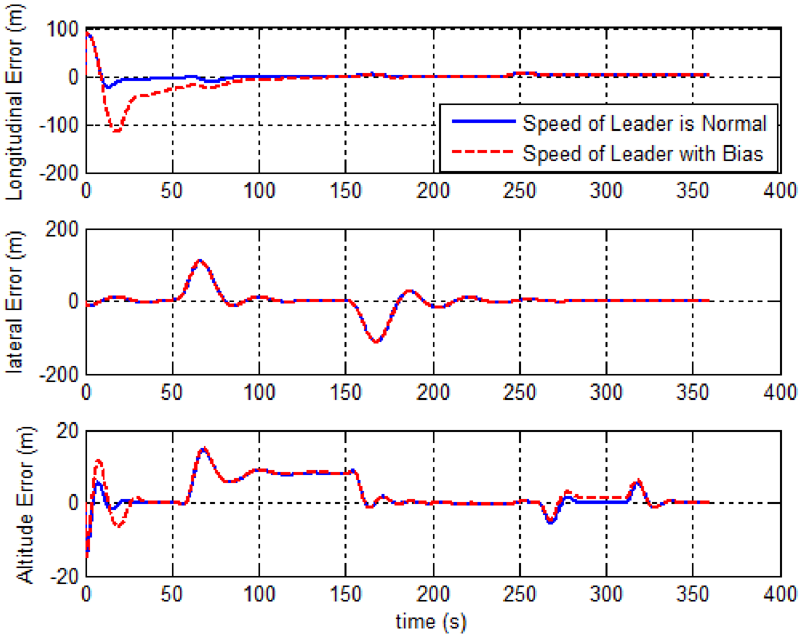

Figure 6.2: Formation results for the case that +20 m/s error in leader's speed with the Lyapunov method

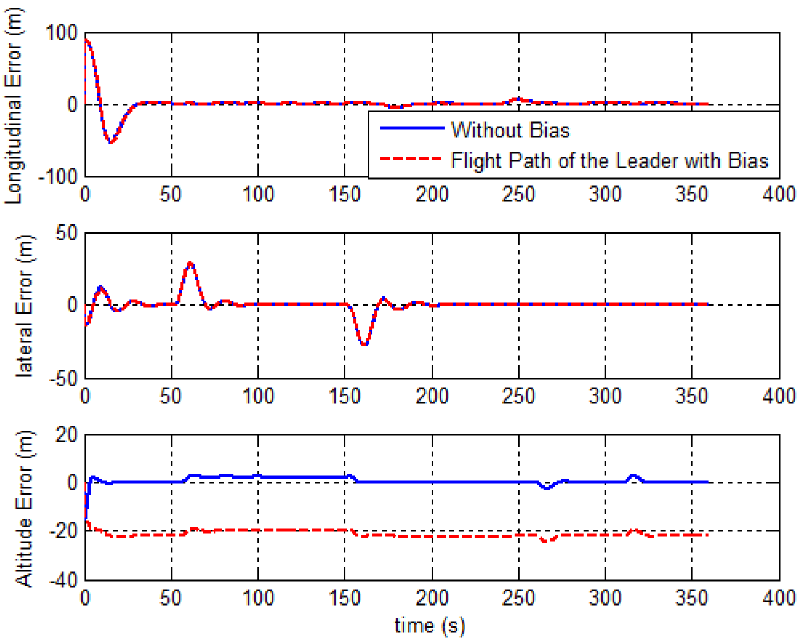

Figure 6.3: Formation results for the case that +2 degree error in leader's flight path angle with the SDRE method

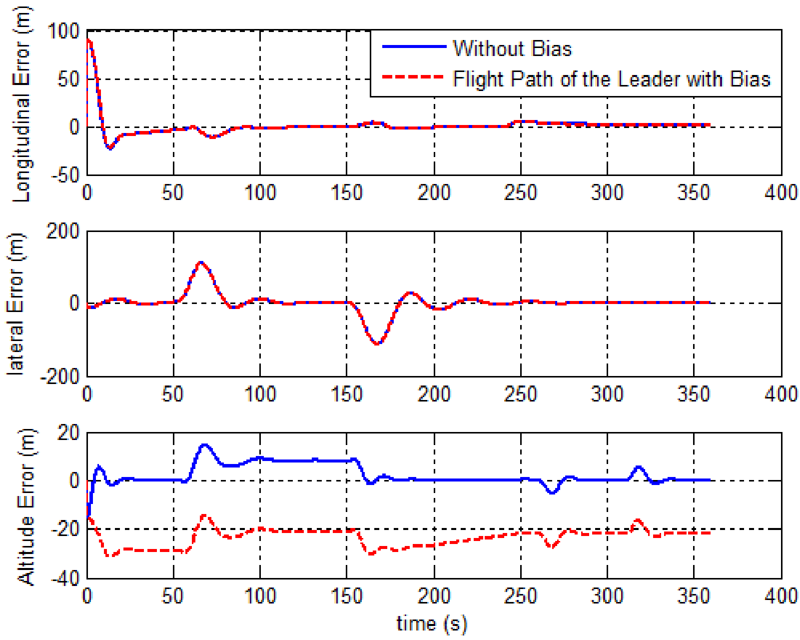

Figure 6.4: Formation results for the case that +2 degree error in leader's flight path angle with the Lyapunov method

6.3 Error in the Heading Rate of the Leader

In this section, heading rate of the leader is given to the follower aircraft as "0". Formation errors are given in Fig. 6.5 for the SDRE based formation controllers. The results show that without leader's heading rate information, follower aircraft can follow the leader perfectly. Same test is conducted on the Lyapunov based controller and the results are given in Fig. 6.6 also show that follower aircraft can track the leader perfectly. Thus, these controllers are insensitive to the yaw rate errors.

6.4 Error in the Heading of the Leader

In this section, when the heading of the leader is taken by the follower aircraft with error is investigated. Simulation results with +5 degree bias, in the leader heading are given in Fig. 6.7 for the SDRE based formation controller. Results show that after some overshoot at the beginning, follower aircraft can track the leader aircraft very well. Moreover, there is not any offset in the lateral channel because integral states of the lateral distance handle that problem.

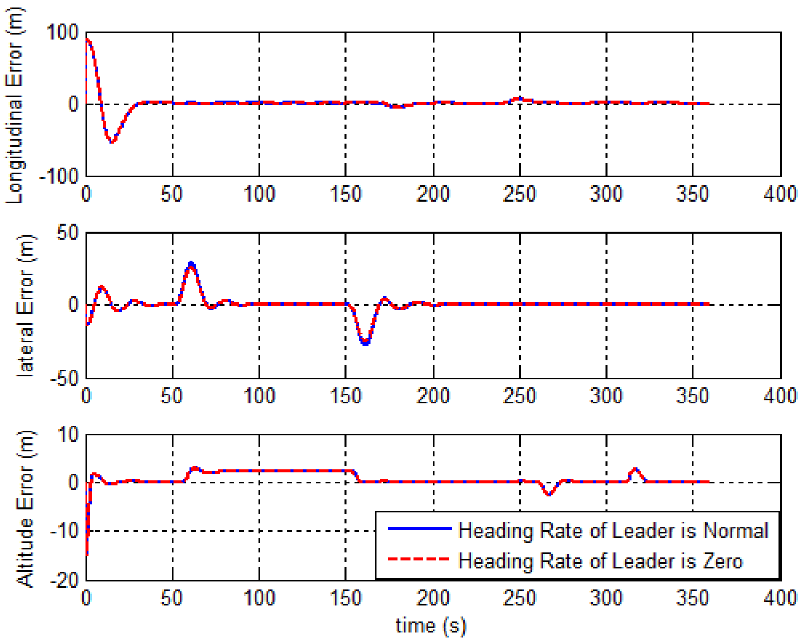

Figure 6.5: Formation results for the case that follower takes the leader's heading rate as "0" with the SDRE method

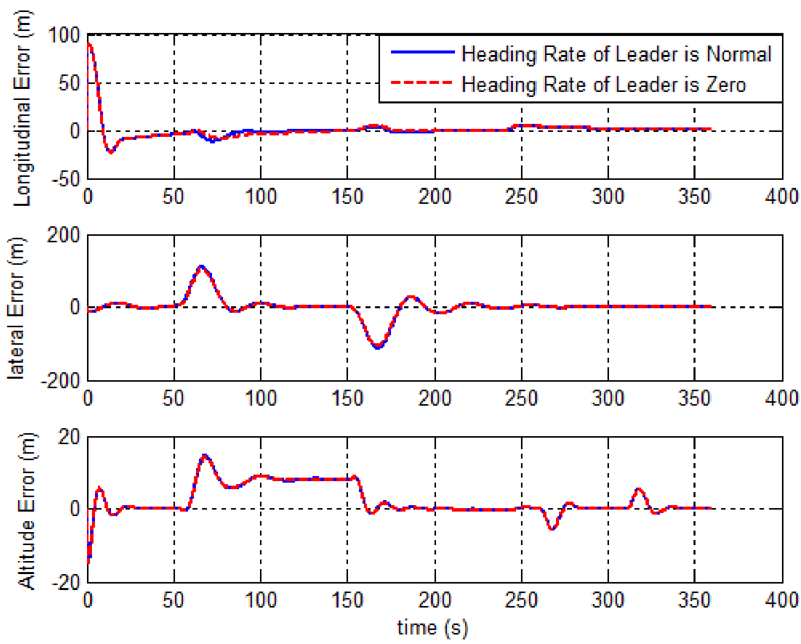

Figure 6.6: Formation results for the case that follower takes the leader's heading rate as "0" with the Lyapunov method

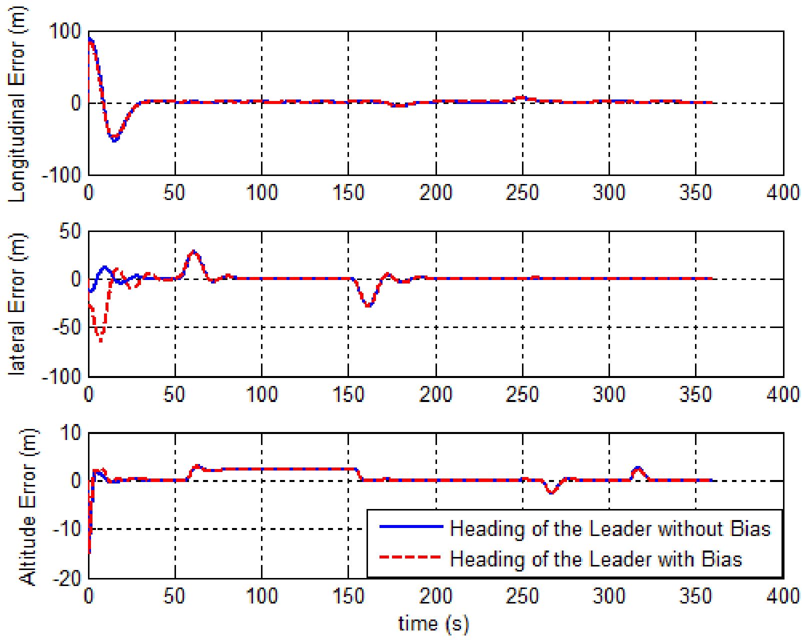

Figure 6.7: Formation results for the case that follower takes the leader's heading with +5 degree bias with the SDRE method

Same test is conducted with the Lyapunov based guidance algorithm and results are given in Fig. 6.8. These results also show that formation controller with Lyapunov method is robust to leader's heading parameter. Thus, the follower can follow the leader aircraft very well with +5 degree heading bias.

6.5 Error in the Positions of the Leader

In this section, when the positions of the leader is taken by the follower aircraft with 30 meter bias is investigated. For the SDRE based formation controller, formation results are given in Fig. 6.9. As expected results show that the follower tracks the leader aircraft with offset in all channel. Same test is conducted with Lyapunov method and results are given in Fig. 6.10. Also, as expected that follower aircrafts follows the leader with the some offset.

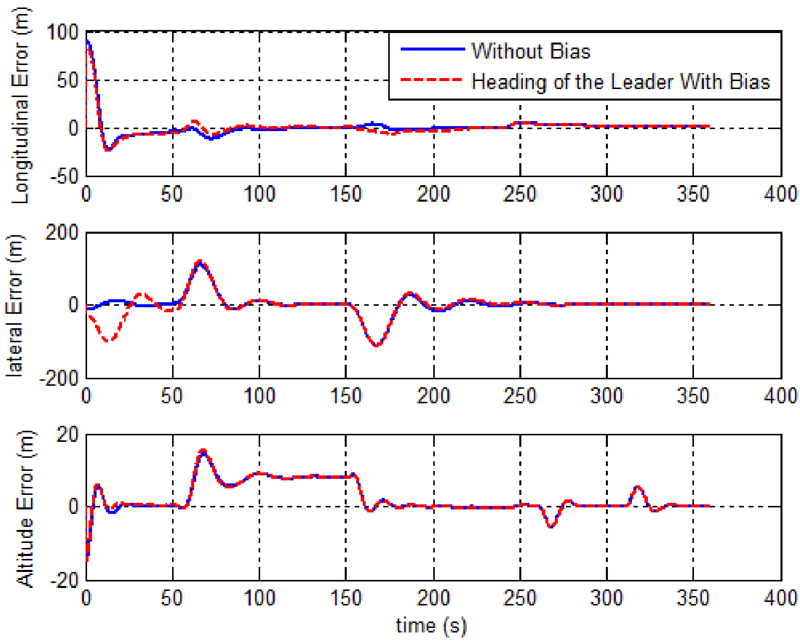

Figure 6.8: Formation results for the case that follower takes the leader's heading with +5 degree bias with the Lyapunov method

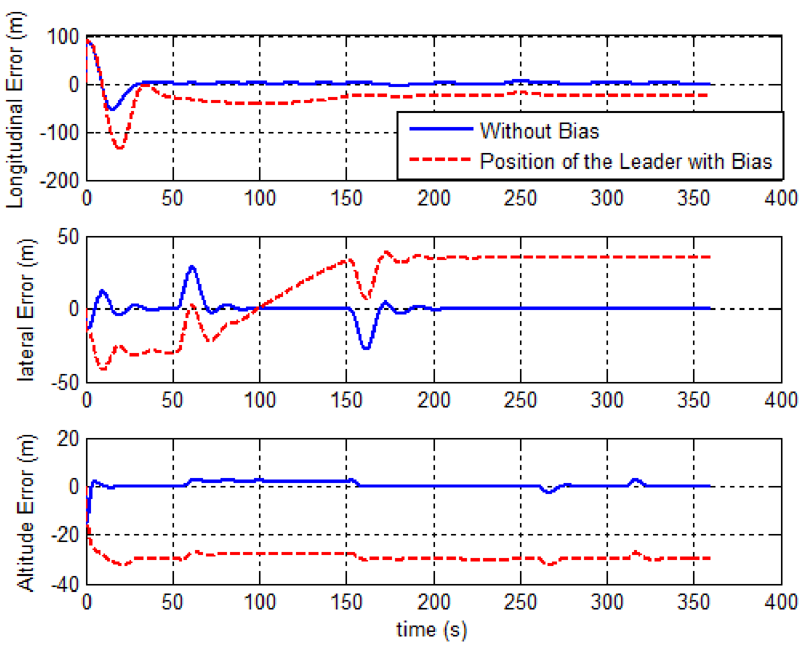

Figure 6.9: Formation results for the case that follower takes the leader's positions with 30 meter bias with the SDRE method

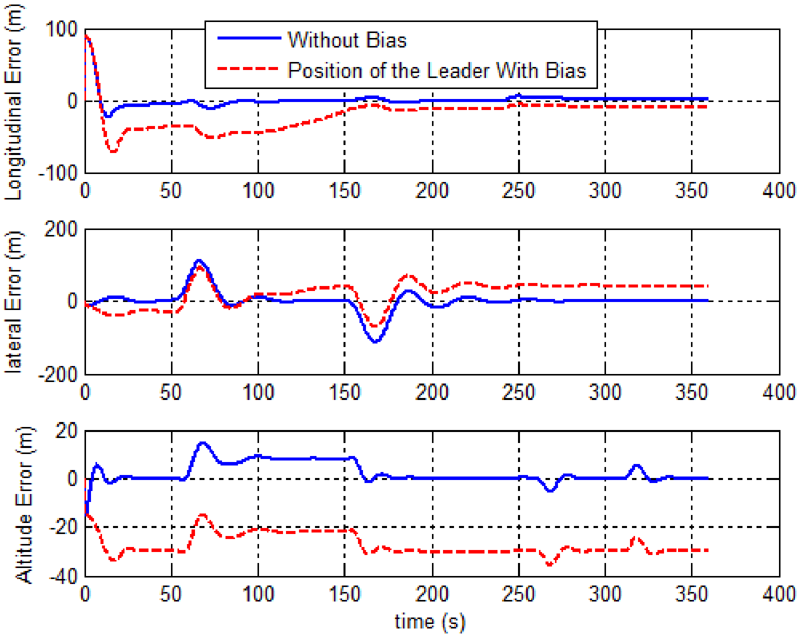

Figure 6.10: Formation results for the case that follower takes the leader's positions with 30 meters bias with the Lyapunov method

CHAPTER 7

COMPARISON AND DISCUSSION BETWEEN THE PROPOSED METHODS

In this study, first formation flight controller is developed with SDRE based method. This method was tested with two different scenario. The difference in these scenarios are flight conditions and maneuvers. Scenario-2 has more rapid maneuvers. In SDRE based formation controller, designed SDRE weights could be used with two different scenarios without changing the weights. However, in Lyapunov function based formation flight controller, that was necessary to tune the weights again. Therefore, it could be an option to design the weights which will depend on some of states for Lyapunov based controller. Thus, the weights can change during flight and this could increase performance of the controller.

In sensitivity analysis, it is showed that both SDRE and Lyapunov based controllers are very robust to observed states of the leader. In simulation tests, it was showed that although the follower took the parameters from leader with some error, it could track the leader aircraft well.

The simulation results show that the proposed two methods can control the formation flight autonomously and they perform very well. It is seen in the simulations that SDRE based formation flight controller has better performance than the Lyapunov function based controller. However, it should be noted that there are lots of parameters that affect the performance of the controllers. Therefore, some other weight choices may improve the performances.

CHAPTER 8

CONCLUSION

In this thesis work, there are two formation flight controllers are proposed. These controllers are developed with SDRE and Lyapunov methods and they are tested in simulations. The simulation results show that proposed algorithms can control the formation flight in Leader-Follower structure autonomously.

On the other hand, SDRE and Lyapunov function based formation flight controllers are tested with given faulty parameters and it is showed that these two controllers are very robust to the taken faulty signals.

Moreover, SDRE based flight controller is developed and it controls the aircraft's speed, heading and altitude. This controller is used in both leader and follower. Therefore, follower aircraft has two loop structure that inner loop has SDRE based flight controller and outer loop has two different types of formation flight controllers. It was also showed that developed inner loops controller with SDRE method can follow the given speed, heading and altitude commands very well.

In this thesis work, vortex model is not modelled. However, in real flight, leader will generate vortex and it will affect the follower aircraft. To make more realistic simulations, vortex will be modelled in future works.

On the other hand, if there are more aircraft or in particular maneuvers in the formation flight, collisions may be a serious problem. Therefore, collision avoidance algorithm shall be added in the future studies.

In this thesis work, proposed algorithms are tested in simulations. However, these methods should be implemented to a model aircraft and real flight test should be conducted.

REFERENCES

[1] B. D. Anderson and J. B. Moore. *Optimal control: linear quadratic methods*. Courier Dover Publications, 2007.

[2] S. ARIYIBI. *NONLINEAR CONTROL OF UNMANNED AIRCRAFT FORMATIONS*. PhD thesis, MIDDLE EAST TECHNICAL UNIVERSITY, 2014.

[3] A. Bogdanov and E. A. Wan. State-dependent riccati equation control for small autonomous helicopters. *Journal of guidance, control, and dynamics*, 30(1):47–60, 2007.

[4] T. Cimen. State-dependent riccati equation (sdre) control: a survey. In *Proceedings of the 17th World Congress of the International Federation of Automatic Control (IFAC), Seoul, Korea, July*, pages 6–11, 2008.

[5] T. Çimen. Systematic and effective design of nonlinear feedback controllers via the state-dependent riccati equation (sdre) method. *Annual Reviews in Control*, 34(1):32–51, 2010.

[6] J. L. Dargan. Proportional plus integral control of aircraft for automated maneuvering formation flight. Technical report, DTIC Document, 1991.

[7] D. Ds and K. Ks. Quaternion based state dependent ricatti equation control of a satellite camera on piezoelectric actuators. 2010.

[8] B. Friedland. *Advanced control system design*. Prentice-Hall, Inc., 1995.

[9] F. R. Garza and E. A. Morelli. A collection of nonlinear aircraft simulations in matlab. *NASA Langley Research Center, Technical Report NASA/TM*, 212145, 2003.

[10] F. Giulietti, L. Pollini, and M. Innocenti. Autonomous formation flight. *Control Systems, IEEE*, 20(6):34–44, 2000.

[11] F. Giulietti, L. Pollini, M. Innocenti, et al. Formation flight control: A behavioral approach. *AIAA paper*, 4239, 2001.

[12] Y. Gu, B. Seanor, G. Campa, M. R. Napolitano, L. Rowe, S. Gururajan, and S. Wan. Design and flight testing evaluation of formation control laws. *Control Systems Technology, IEEE Transactions on*, 14(6):1105–1112, 2006.

[13] N. Li and H. Liu. Multiple uavs formation flight experiments using virtual structure and motion synchronization. In *AIAA Guidance, Navigation and Control Conference, Chicago*, 2009.

[14] P. Menon, T. Lam, L. Crawford, and V. Cheng. Real-time computational methods for sdre nonlinear control of missiles. In *American Control Conference, 2002. Proceedings of the 2002*, volume 1, pages 232–237. IEEE, 2002.

[15] C. P. Mracek and J. R. Cloutier. Missile longitudinal autopilot design using the state-dependent riccati equation method. Technical report, Embry-Riddle Aeronautical Univ. Press, Daytona Beach, FL (United States), 1994.

[16] D. S. Naidu. *Optimal control systems*, volume 2. CRC press, 2002.

[17] M. Pachter, J. J. D', Azzo, and A. W. Proud. Tight formation flight control. *Journal of Guidance, Control, and Dynamics*, 24(2):246–254, 2001.

[18] J. Pearson. Approximation methods in optimal control i. sub-optimal control†. *International Journal of Electronics*, 13(5):453–469, 1962.

[19] A. Prach and O. Tekinalp. Development of a state dependent ricatti equation based tracking flight controller for an unmanned aircraft. In *Proc. AIAA Guidance, Navigation, and Control Conference, Boston, MA*, 2013.

[20] B. L. Stevens and F. L. Lewis. *Aircraft control and simulation*. John Wiley & Sons, 2003.

[21] O. Tekinalp and S. Kumbasar. Sdre based guidance and flight control of aircraft formations. In *AIAA, SciTech 2015, Orlando, FL, January 5-9, 2015.*

[22] A. Wernli and G. Cook. Suboptimal control for the nonlinear quadratic regulator problem. *Automatica*, 11(1):75–84, 1975.

[23] D. I. You and D. H. Shim. Autonomous formation flight test of multi-micro aerial vehicles. *Journal of Intelligent & Robotic Systems*, 61(1-4):321–337, 2011.